FIBER REINFORCED GEOPOLYMER COMPOSITES SUITABLE FOR ADDITIVE MANUFACTURING

ÜÇ BOYUTLU EKLEMELİ İMALATA UYGUN LİF DONATILI JEOPOLİMER KOMPOZİTLER

Ehsan Aminipour

PROF. DR. MUSTAFA ŞAHMARAN

Supervisor

Submitted to

Graduate School of Science and Engineering of Hacettepe University

as a Partial Fulfillment to the Requirements

for be Award of the Degree of Master of Science

in Civil Engineering

2023

ABSTRACT

FIBER REINFORCED GEOPOLYMER COMPOSITES SUITABLE FOR ADDITIVE MANUFACTURING

Ehsan Aminipour

Master of Science, Department of Civil Engineering

Supervisor: Prof. Dr. Mustafa ŞAHMARAN

July 2023, 91 pages

The conventional use of traditional concrete, especially Portland cement, has given rise to a multitude of environmental and sustainability concerns. One such concern is the significant contribution of Portland cement to global CO_2 emissions, which is estimated to be around 8-9% worldwide. Given the escalating demand for concrete driven by the need for shelter and transportation, it is imperative to identify a new, sustainable, and eco-friendly alternative to traditional concrete production. In addition to the environmental impact of Portland cement, the management and recycling of construction demolition waste present another challenge for humanity. Construction demolition waste accounts for approximately one-third of the total annual waste in the European Union, and the rates of reuse vary depending on the economic strength of countries. Moreover, countries with larger economies face limitations in producing value-added goods through the reuse of construction demolition waste, so effectively addressing these material-related issues is of utmost importance. Furthermore, the traditional production methods employed in the construction industry are often slow, risky, and costly, especially in the face of modern technology. Occupational accidents associated with molded construction processes are a significant concern. Mold and labor costs also need to be optimized during the production stages. This thesis sets out to

explore the impact of various fiber types on the creation of innovative and eco-friendly 3D printable geopolymer-based composites. Delving into this subject, thorough examinations have been conducted to uncover the mechanical properties, such as flexural strength, inter-layer bond strength, and compressive strength of extrusion-based 3D printed geopolymer composites. These investigations involve assessing the properties of cured mixtures over different durations under ambient conditions.

The envisioned outcome of these composite materials goes beyond conventional benefits. Notably, they strive to combat the detrimental effects of cement production on the environment, revolutionize the reuse of construction demolition waste by adding value to it, and revolutionize the construction industry through 3D production automation. Anticipated as a groundbreaking step, the development of geopolymer composites tailored for 3D-AM technology offers a beacon of hope in addressing several pressing challenges faced by the construction industry. These include mitigating global warming, alleviating excessive costs, curbing occupational accidents, and devising better solutions for construction demolition waste management.

Through this journey of exploration, the thesis seeks to present captivating solutions that promise to revolutionize the construction landscape and contribute to a more sustainable and eco-friendly future.

Keywords: 3D printing, fiber reinforced geopolymer, construction and demolition waste, geopolymer, anisotropy, alkaline content, bond strength.

ÖZET

ÜÇ BOYUTLU EKLEMELİ İMALATA UYGUN LİF DONATILI JEOPOLİMER KOMPOZİTLER

Ehsan Aminipour

Yüksek Lisans, İnşaat Mühendisliği Bölümü
Tez Danışmanı: Prof. Dr. Mustafa ŞAHMARAN
Temmuz 2023, 91 sayfa

Geleneksel betonun, özellikle Portland çimentosunun geleneksel kullanımı, çok sayıda çevresel ve sürdürülebilirlik sorunuyla sonuçlanmıştır. Bu, Portland çimentosunun dünya çapında yaklaşık %8-9'a tekabül eden küresel CO_2 emisyonlarına önemli katkısını içerir. İnsanların barınma ve ulaşım ihtiyaçları nedeniyle betona olan talep artmaya devam ederken, geleneksel beton üretimine yeni, sürdürülebilir ve çevre dostu bir alternatif bulmak çok önemlidir.Portland çimentosunun çevresel etkisine ek olarak, inşaat yıkım atıklarının depolanması ve geri dönüştürülmesi insanlık için başka bir zorluk oluşturmaktadır. Avrupa Birliği'ndeki yıllık toplam atığın yaklaşık üçte birini inşaat yıkım atıkları oluşturuyor ve ülkelerin ekonomik gücüne bağlı olarak değişen yeniden kullanım oranları var. Büyük ekonomiye sahip ülkelerde inşaat yıkım atıklarının yeniden kullanılması yoluyla katma değerli mal üretimi de sınırlıdır. Malzemeyle ilgili bu sorunların ele alınması esastır. Ayrıca, inşaat sektöründe kullanılan geleneksel üretim yöntemleri, özellikle modern teknoloji karşısında genellikle yavaş, riskli ve maliyetlidir. Kalıplanmış inşaat süreçleriyle ilgili iş kazaları önemli bir endişe kaynağıdır. Üretim aşamalarında kalıp ve işçilik maliyetlerinin de optimize edilmesi gerekiyor. Bu tez, yenilikçi ve çevre dostu 3D yazdırılabilir jeopolimer bazlı kompozitlerin oluşturulmasında çeşitli elyaf türlerinin etkisini keşfetmeyi amaçlamaktadır. Bu konuyu derinlemesine inceleyerek, ekstrüzyon tabanlı

3D baskılı jeopolimer kompozitlerin eğilme dayanımı, katmanlar arası bağ dayanımı, basınç dayanımı ve anizotropik davranışı gibi mekanik özelliklerini ortaya çıkarmak için kapsamlı incelemeler yapılmıştır. Bu araştırmalar, kürlenmiş karışımların özelliklerinin, ortam koşulları altında farklı süreler boyunca değerlendirilmesini içerir.

Bu kompozit malzemelerin öngörülen sonucu, geleneksel faydaların ötesine geçiyor. Özellikle, çimento üretiminin çevre üzerindeki zararlı etkileriyle mücadele etmek, inşaat yıkım atıklarına değer katarak yeniden kullanımında devrim yaratmak ve 3D üretim otomasyonu yoluyla inşaat endüstrisinde devrim yaratmak için çabalıyorlar. Çığır açan bir adım olarak beklenen, 3D-AM teknolojisi için özel olarak tasarlanmış jeopolimer kompozitlerin geliştirilmesi, inşaat endüstrisinin karşı karşıya olduğu çeşitli acil zorlukların ele alınmasında bir umut ışığı sunuyor. Bunlar arasında küresel ısınmayı azaltmak, aşırı maliyetleri azaltmak, iş kazalarını azaltmak ve inşaat yıkım atık yönetimi için daha iyi çözümler bulmak yer alıyor.

Bu keşif yolculuğu boyunca tez, inşaat alanında devrim yaratmayı ve daha sürdürülebilir ve çevre dostu bir geleceğe katkıda bulunmayı vaat eden büyüleyici çözümler sunmayı amaçlıyor.

Anahtar Kelimeler: 3D baskı, fiber takviyeli geopolimer, inşaat ve yıkım atıkları, geopolimer, anizotropi, alkali içeriği, bağ kuvveti.

ACKNOWLEDGEMENT

I would like to express my deepest gratitude and appreciation to all those who have supported me during the completion of this thesis. Their unwavering encouragement, guidance, and assistance were instrumental in its successful completion.

First and foremost, I would like to express my sincere gratitude to my supervisor, Prof. Dr. Mustafa ŞAHMARAN, for their invaluable guidance, expertise, and continuous support. Their insightful feedback, patience, and encouragement have been instrumental in shaping this thesis and enhancing its quality. I am truly grateful for their mentorship and the trust they placed in me.

I am also indebted to the members of my thesis committee, Prof. Dr. İlhami Demir, Assoc. Dr. Gürkan Yıldırım, Assoc. Dr. Mustafa Kerem Koçkar and Asst. Dr. Hüseyin Ulugöl for their expertise, constructive criticism, and valuable suggestions. Their insightful comments and recommendations have immensely contributed to refining the scope and content of this work.

I am grateful to the staff and faculty of the civil engineering department at Hacettepe University for their crucial resources and facilities. Special thanks to Hüseyin İLCAN, Merve SÖNMEZ TUĞLUCA, and Emircan ÖZÇELİKCİ for their valuable time and insights in gathering the necessary data for this study.

Furthermore, the author gratefully acknowledges the financial assistance of the Scientific and Technical Research Council (TUBITAK) of Turkey provided under Project: 119N030.

Lastly, heartfelt thanks to my family and friends, especially my father Hossein Aminipour, for their unwavering support and belief in me. Their encouragement has been a constant inspiration throughout this journey.

Ehsan Aminipour

July 2023, Ankara

TABLE OF CONTENTS

ABSTRACT i
ÖZET iii
ACKNOWLEDGEMENT v
TABLE OF CONTENTS vi
LIST OF FIGURES viii
LIST OF TABLES x
SYMBOLS AND ABBREVIATIONS xi
1. INTRODUCTION 1
1.1 General 1
1.2 Research Targets and Purpose 4
1.3 Thesis Outline 5
2. LITERATURE RESEARCH 7
2.1 Geopolymer Binder Systems 7
2.2 Construction Industry Automated Fabrication/AM 16
2.2.1 The historical background of AM Technology 16
2.2.2. Reinforcement in 3D-Printing with Fiber Inclusion. 21
3. MATERIALS AND METHODOLOGY 26
3.1 Materials 26
3.1.1. Materials in the Making 26
3.1.1.1. CDW Materials 26
3.1.1.2 Blast Furnace Slag (BFS) 33
3.1.2 Alkaline Activators 34
3.1.2.1. Sodium Hydroxide (NaOH) 34
3.1.2.2. Calcium Hydroxide 35
3.1.3 Recycled Concrete Aggregate (RCA) 36
3.1.4 Fibers 37
3.1.4.1 Waste Wood Fibers (WWF) 37
3.1.4.2 Polyvinyl Alcohol (PVA) Fiber 38
3.1.4.3 Polypropylene (PP) Fiber 39
3.2. Methodology 39

3.2.1. Mixture Preparation Process 40
3.2.2. Specimen Fabrication 41
3.2.2.1. Mixture Properties 41
3.2.2.2. Casting Process 43
3.2.2.3. Three-Dimensional Additive Manufacturing Process 44
3.2.3 Testing 45
3.2.3.1 Flexural Strength Testing 45
3.2.3.2 Compressive Strength Testing 47
3.2.3.3 Interlayer Bond Strength 48
3.2.4 Alkali Treatment Protocol 50
4. RESULTS AND DISCUSSION 52
4.1 Optimizing WWF Ratios for Casted Geopolymer 52
4.2 Optimizing PVA Fiber Lengths for Casted Geopolymer 55
4.3 Optimizing PVA Fiber Ratios for Casted Geopolymer 57
4.4 Optimizing PP Fiber Ratios for Casted Geopolymer 61
4.5 Compressive Strength 63
4.5.1 Effect of WWF on the Compressive Strength 63
4.5.2 Effect of PVA Fiber on the Compressive Strength 66
4.5.3 Effect of PP Fiber on the Compressive Strength 67
4.6 Flexural Strength 68
4.6.1 Effect of Various Fibers on Flexural Strength 70
4.6.2 Mechanical Properties Dependent on Direction 71
4.7 Direct Tensile Strength 72
5. CONCLUSIONS 75
6. REFERENCES 80

LIST OF FIGURES

Figure 2.1. Schematic illustration of the formation of geopolymer monomers [28][29]..9
Figure 2.2. Illustration depicting the Polymerization schematic for geopolymer [28]. 9
Figure 2.3. Structure of geopolymer [30].....10
Figure 2.4. Model of geopolymerization processing [36][37]. 11
Figure 2.5. Model of geopolymerization for alkali-activated system [39].....12
Figure 3.1. Jaw crusher. 27
Figure 3.2. Ball mills in Research: visual compilation. 27
Figure 3.3. Raw, crushed, and grinding phases of the CDW materials. 28
Figure 3.4. The distribution of particle sizes in the precursor materials[57]. 30
Figure 3.5. CDW-based precursor SEM micrographs[54].....31
Figure 3.6. XRD models of CDW-based precursors.....33
Figure 3.7. Blast Furnace Slag Powder. 34
Figure 3.8. Flaked format of NaOH. 35
Figure 3.9. Calcium Hydroxide powder.....36
Figure 3.10. From left to right, the raw, crushed, and grinding phases of the RCA. 37
Figure 3.11. Polyvinyl alcohol (PVA) fiber. 38
Figure 3.12. Polypropylene (PP) fiber. 39
Figure 3.13. Adding WWF– Polypropylene (PP) fiber to mixture. 41
Figure 3.14. 50x50x50 mm^3 empty and poured cubic molds.....43
Figure 3.15. 240x80x15 mm^3 empty and poured cuboid rectangular prism molds. 43
Figure 3.16. Specifics on the lab-scale 3D printer. 44
Figure 3.17. The preparation of the specimens involved (A) utilizing two-ply filaments and (B) cutting fresh filaments.....45
Figure 3.18. General Schematic View Flexural Strength of 3D-Printed Sample[57].....46
Figure 3.19. Images of prismatic samples under various loading circumstances. 47
Figure 3.20. General view of printed specimens for 3 types of compressive stress[57].48
Figure 3.21. From left to right, T-shaped metal profile, glued profile, glued sample.....48
Figure 3.22. Sample subjected to direct tensile stress.....49
Figure 3.23. Process of immersing WWFs in an alkali solution.....50
Figure 3.24. Untreated WWF and the WWF treated with alkali.....51

Figure 4.1. Flexural strength-displacement graph of 7-day-old specimens with varying WWF percentages. 53
Figure 4.2. Flexural strength-displacement graph of 28-day-old specimens with varying WWF percentages. 55
Figure 4.3. Flexural Strength-Displacement Graph for PVA Fiber (6.00, 8.00, 12.00 mm, 0.50% and 1.00% volume) at 28-day. 56
Figure 4.4. Flexural strength-displacement graph of 7-day-old PVA fiber (6.00mm length) with volume percentages of 0.25%, 0.50%, 0.75%, and 1.00%. 59
Figure 4.5. Flexural strength-displacement graph of 28-day-old PVA fiber (6.00mm length) with volume percentages of 0.25%, 0.50%, 0.75%, and 1.00%. 59
Figure 4.6. Flexural strength-displacement graph of 7-day-old PP fiber (6.00mm length) with volume percentages of 0.25%, 0.50%, 0.75%, and 1.00%. 61
Figure 4.7. Flexural strength-displacement graph of 28-day-old PP fiber (0.25%, 0.50%, 0.75%, 1.00% volume). 63
Figure 4.8. Compressive strength of 7-day and 28-day samples (Plain, 2.00% WWF). 65
Figure 4.9. 7-day and 28-day compressive strength of samples (Plain, 0.50% and 0.75% PVA). 67
Figure 4.10. 7-day and 28-day compressive strength of geopolymer samples (Plain, 0.50% and 0.75% PP). 68
Figure 4.11. Flexural strength of 3D-printed samples (WWF, PVA, PP fiber combinations)..... 69
Figure 4.12. Direct tensile strength of 3D-printed samples (WWF, PVA, PP combinations)..... 73

LIST OF TABLES

Table 3.1. Outcome of XRF analysis [54]. 29
Table 3.2. The XRD investigations yielded chemical formulas and assigned Powder Diffraction File (PDF) numbers for the crystalline phases 33
Table 3.3. Geopolymer mortar mixture proportions. 42

SYMBOLS AND ABBREVIATIONS

Symbols

τ	Flowability Index
℃	Centigrade Degree

Abbrevetions

$(OH)^-$	Hydroxide Ion
3D	There-Dimensional
3D-AM	Three-Dimensional Additive Manufacturing
Al	Aluminum
BW	Brick Waste
$Ca(OH)_2$	Calcium Hydroxide
CASH	Calcium Silica Alumina Hydrate
CDW	Construction and Demolition Waste
CSH	Calcium Silica Hydrate
CW	Concrete Waste
FA	Fly Ash
FTIR	Fourier Transform Infrared Spectroscopy
GBFS	Granulated Blast-Furnace Slag
GW	Glass Waste
HB	Hollow Brick
K_2O_3Si	Potassium Silicate
KOH	Potassium Hydroxide
MK	Metakaolin
MR	Molar Ratio

Na	Normal Aggregate
Na_2SiO_3	Sodium Silicate
NaOH	Sodium Hydroxide
OPC	Ordinary Portland Cement
PBO	Polyphenylene Benzobisoxazole
PC	Portland Cement
PDF	Powder Diffraction File
PP	Polypropylen
PVA	Polyvinyl Alcohol
RCA	Recycled Concrete Aggregate
RCB	Red Clay Brick
RT	Roof Tile
S/B	Solution to Binder Ratio
SEM	Scanning Electron Microscopy
Si	Silicon
W/B	Water to Binder Ratio
XRD	X-Ray Diffraction
XRF	X-Ray Fluorescence

1. INTRODUCTION

1.1 General

Throughout history, human needs have remained relatively consistent. The fundamental requirements for shelter, organization, communication, and protection from the elements have always been essential. Consequently, the utilization of materials to fulfill these needs has been a constant practice, with concrete emerging as a primary choice for centuries. Concrete has been extensively employed in constructing diverse structures such as buildings, bridges, roads, and other infrastructure, and its popularity endures due to the numerous advantages it offers. Notably, concrete excels in its capacity to endure challenging weather conditions, including extreme temperatures and moisture, making it a highly desirable construction material [1]. This makes it ideal for use in outdoor construction projects, as well as in areas prone to earthquakes or other natural disasters. In addition to its strength and durability, concrete is also widely used because it is relatively inexpensive and easy to work with. It can be molded and shaped into a variety of forms, and it is relatively simple to mix and pour on-site. It is therefore a sensible option for a variety of building jobs. However, as result of that the energy intensity for the production procedure of the key component of concrete namely cement is noticeably high and it entails carbon dioxide (CO_2) emissions resulting from the chemical reaction triggered during its process, which in turn accounts for the emission of global greenhouse gases. The estimations generated by the International Energy Agency indicate that the cement sector is one of the major industrial producers of CO_2 emissions, contributing around 8% of the world's total CO_2 emissions[2].

There are multiple ways that cement manufacturing contributes to CO_2 emissions. Burning energy sources like natural gas, oil, and coal derived from fossil fuels to create the heat necessary to build cement is an integral part of one of those approaches. The chemical reaction that occurs during the production of cement, known as the "decarbonation" of limestone, also releases CO_2. In addition, the transportation of raw materials and finished cement products can also contribute to CO_2 emissions. Also, concrete production can result in the emission of several types of air pollutants, in addition to CO_2. Some of the specific pollutants that may be emitted during the production of concrete include; Nitrogen oxide (NOx) emissions can

originate from the combustion of energy sources including natural gas, oil, and coal. When fossil fuels containing sulfur are burned, it generates sulfur dioxide (SO_2), which is a gas. Similarly, the burning of fossil fuels produces carbon monoxide (CO), a colorless and odorless gas. Particulate matter, on the other hand, refers to tiny solid or liquid particles suspended in the air [3][4][5]. Apart from the aforementioned air pollutants, the manufacturing process of concrete can also lead to the creation of waste materials such as slag and FA, which require appropriate disposal methods. Furthermore, there has been a substantial global rise in cement production, reaching 4.4 billion tons in 2022 compared to just 0.94 billion tons in 1970 [6]. It is anticipated to reach a startling 5.9 billion tons by 2050 if alternative binders are not introduced [7]. Natural resources, including clay, limestone, and water, must be used in the cement manufacturing process. The production process, which involves the grinding and heating of a combination of limestone, clay, and sand, depends heavily on these resources. The usage of natural resources in the manufacture of cement may prove detrimental to the environment, including the depletion of water resources and the extraction of limestone and clay from the earth, which can lead to habitat destruction and degradation. To mitigate these impacts, it is important for cement producers to adopt sustainable practices that reduce the environmental effect of cement manufacturing by minimizing the usage of natural resources.

An unintended consequence that arises from the production of concrete is construction and demolition waste (CDW) as it is often not properly managed and can contribute to significant environmental problems, pollution, and land degradation [8][9][10]. Moreover, CDW contains valuable resources such as metal, wood, and concrete that have the potential to be recycled or reused. Consequently, there is an increasing effort to redirect CDW away from landfills and promote the recycling and reuse of these materials. CDW can make up a significant portion of total waste, depending on the region and the waste management practices in place. Based to the Environmental Protection Agency (EPA) of the United States, CDW made up about 29% of total non-industrial waste in the U.S. in 2017 [11]. However, this figure can vary significantly from one region to another and can be influenced by factors such as the level of economic development, the prevalence of construction activities, and the effectiveness of waste management programs. In some regions, CDW may make up a much smaller or larger proportion of total waste.

Geopolymer made from concrete and demolition waste, also known as CDW-based geopolymer, is a type of construction material that is produced by mixing CDW with an alkaline solution to make a solid, strong material. CDW-based geopolymer can potentially substitute the conventional cement-based concrete as it has several potential benefits. One potential benefit of CDW-based geopolymer is that it will result in a smaller amount of waste left behind following construction and demolitions process. Using CDW as a raw material in geopolymer manufacture offers a viable alternative for mitigating the environmental effects of the massive quantity of waste created globally. CDW-based geopolymer may have a lower carbon footprint than traditional concrete. The cement produce, as the key component of conventional concrete, accounts for greenhouse gas emissions. The utilization of CDW as a fundamental component in geopolymer manufacture offers a possible option for mitigating the carbon emissions generally connected with the fabrication of building materials. CDW-based geopolymer has the potential to be a sustainable and environmentally friendly alternative to conventional cement-based concrete in the industries related to construction.

The remarkable advancement of 3D-printing technology, is that this technology revolutionized diverse industries ranging from manufacturing to medicine, propelling them forward with unprecedented possibilities. The construction industry is one of the industries that have been affected by this technology. 3D printing in construction is discovered to be very promising to address the accommodation shortage problem and the high cost of its construction. 3D-AM, or 3D Additive Manufacturing, refers to a range of technologies that involve building up physical objects layer by layer using 3D printing or other additive manufacturing techniques. These innovative technologies have the capacity to transform the construction sector by facilitating the swift and economical manufacturing of intricate structures and building elements.

3D-AM in construction offers a notable advantage in its capability to fabricate customized shapes and intricate geometries, surpassing the limitations of conventional manufacturing techniques. This can lead to more efficient and effective construction processes, as well as the development of new designs and building concepts [12]. 3D-AM in construction also brings the advantage of waste reduction and enhanced sustainability. Unlike traditional construction

methods that generate substantial waste materials, 3D-AM minimizes waste production, leading to cost savings in waste disposal and mitigating environmental harm [13][14]. In contrast, 3D-AM allows for precise control over the production process, enabling the production of only the necessary material and reducing waste. 3D printing offers a range of advantages over traditional construction methods, including increased speed, reduced costs, and improved sustainability. The automation of housing construction through 3D printers is expected to be a prominent application of this technology, alongside its uses in fields such as medicine, education, prototyping and manufacturing, as well as art and jewelry. This versatile technology has the potential to revolutionize various industries and enable innovative solutions to complex challenges. The housing sector can benefit from various advantages, such as the ability to create intricate and precise structures, accelerated construction processes, reduced labor expenses, and decreased waste in the form of discarded construction materials like scrap wood and metal [15][16].

With the rising demand for housing and the scarcity of skilled labor, the use of 3D printing in construction offers a significant advantage by minimizing the reliance on human workforce. By employing 3D printers, intricate structures and high-resolution components can be produced with comparable speed to conventional manufacturing techniques. This advancement addresses the labor shortage challenge and enables the construction industry to meet the growing housing needs effectively [17].

1.2 Research Targets and Purpose

This research aimed to mitigate the adverse ecological and environmental effects of CDWs while exploring their potential applications in 3D printing. By integrating CDW-based mortar with 3D printing technology, the construction industry can benefit from advantages such as enhanced customization, reduced construction time, decreased labor requirements, and lowered costs. The CDW-based geopolymer composite utilized in this study was derived from recycled materials such as hollow bricks (HB), red clay bricks (RCB), roof tiles (RT), glass waste (GW), and concrete waste (CW). However, this geopolymer composite exhibits certain limitations, including low flexural and tensile strength, which restrict its widespread adoption in various applications. The main objectives of this research are to improve the mechanical

properties of CDW-based geopolymer binders as a sustainable alternative to cement, a significant source of CO_2 emissions. To accomplish these objectives, the focus of this thesis lies in evaluating the feasibility of reinforcing geopolymer mortars through the incorporation of different fiber types into the mixtures. The investigation primarily examines the mechanical and bond strength properties of reinforced with different fiber types and ratios of geopolymer mixtures composed of CDW. Detailed descriptions of the methodology employed throughout the study are presented in the subsequent sections.

The primary objective of this study is to investigate the impact of incorporating diverse natural and synthetic fibers on the mechanical properties of the geopolymeric system. To achieve this goal, waste wood fiber (WWF) is selected as the natural fiber, while polyvinyl alcohol (PVA) and polypropylene (PP) fibers are chosen as the synthetic fibers. The experimental phase of the research encompasses conducting compressive strength tests, flexural strength tests, and direct tensile examinations to assess the performance of the geopolymeric system.

To assess the fiber reinforcing on 3D-printed samples, thorough evaluations were conducted. The experimental protocol encompassed subjecting the samples to compressive strength assessments along three unique loading directions, while 3-point bending system tests were conducted in two separate loading directions. To assess the effectiveness of fiber inclusion on mechanical characteristic of 3D-printed geopolymeric composites, a comparative analysis was performed by conducting testing under flexural and compressive loading. Additionally, the bonding strength of the printed specimens were decided using direct tensile tests.

1.3 Thesis Outline

The following is a list of the 5 stages that make up the details of this thesis.
In the first part of the thesis, titled "Introduction", an overview of the study is provided, including the main problems addressed and solutions proposed. The specific goals of the study are also outlined in detail.

The second part of the document, called "Literature Review", discusses research that has been conducted in recent years on the creation of geopolymer. Additionally, it discusses the

application of geopolymer in 3D-AM technology, 3D technologies, and automation in the construction sector.

The third section, "Materials and Methods", which presents comprehensive details about the substances employed in the study, including precursors, alkali activators, recycled aggregate, and fibers. This section also elucidates the testing techniques used to assess properties of the innovative environmentally-friendly materials. Additionally, it provides an in-depth account of the specific 3D printer utilized in the research, along with a thorough explanation of the printing process that was employed.

The "Results and Discussion" section, positioned as the fourth segment, presents an in-depth analysis of the compressive/flexural/bond strength between layers of mixtures comprised of CDW materials. Moreover, the influence of fibers at these properties is thoroughly examined. This section provides a comparative assessment of the mechanical attributes between 3D-printed samples and those fabricated using traditional manufacturing techniques, while exploring the underlying factors contributing to these outcomes. Additionally, the examination extends to the mechanical parameters, such as flexural strength, compressive strength, and interlayer bond strength, considering the variations in fiber types and lengths.

In the final segment titled "Conclusion," the intriguing findings derived based on the experimental research done for the thesis are consolidated and presented concisely.

2. LITERATURE RESEARCH

Concrete is used abundantly in the modern world, second only to water [18][19]. The annual consumption of concrete worldwide is around 25 Gigatons, which translates to an average usage of 3.8 tons per person per year [20]. The consumption of concrete is also on the rise globally and is anticipated to maintain this trend because of the continuous construction activities taking place in developing nations [21]. Despite its widespread use, concrete poses significant challenges, particularly due to the negative environmental impact associated with Portland cement (PC). PC, as a primary binding material in conventional concrete, has garnered considerable attention and concern due to its substantial energy consumption during production, leading to the emission of significant amounts of greenhouse gases [22]. Moreover, the extensive utilization of clean water, clay, limestone, variously-sized aggregates, and gypsum in the production of PC and concrete further exacerbates the environmental implications [23]. It can be vividly concluded that having the collective interest of the environment, economy, and society in mind and due to the aforementioned repercussions, a number of measures should be taken to cut down on the use of cementitious materials. In the pursuit of sustainable construction practices, researchers have been dedicated to discovering alternative construction materials that prioritize environmental friendliness and reduce energy and resource consumption [24][25]. Through these endeavors, a groundbreaking creation of alkali-activated materials, also known as geopolymers, a type of binder material, has emerged as a result. These innovative materials signify a significant step forward in construction technology. These materials have been successful as partial or complete alternatives for Portland cement.

2.1 Geopolymer Binder Systems

Geocements (GCs) are a form of cementitious material with an alumino-silicate composition. They are produced through a chemical process known as "geopolymerization," which involves the interaction of solid alumino-silicate precursors with solutions containing alkali hydroxides or silicates, such as potassium hydroxide (KOH), sodium hydroxide (NaOH), potassium silicate (K_2SiO_3), sodium silicate (Na_2SiO_3). Geopolymers can exhibit diverse characteristics

depending on the materials utilized during production. These characteristics may include reduced thermal conductivity, resistance to fire and acids, varying setting times, and enhanced strength. The utilization of repurposed industrial and construction waste as raw materials for geopolymers eliminates significant costs, making them a feasible and cost-effective binding material. In 1980, Joseph Davidovits made significant contributions to the field by introducing scientific research on geopolymer materials and pioneering the development of the first inorganic polymer [26]. In an exciting breakthrough, a process called geopolymerization has been introduced, revolutionizing the construction landscape. This process entails the fusion of abundant natural minerals, such as fly ash, clay, slag, and pozzolan, which are abundance of silicon (Si) and aluminum (Al), with the aid of an alkaline activator. Notably, this geopolymerization process occurs at temperatures below 160°C. Geopolymerization refers to the alkali activation of alumina-silicates, which involves transforming amorphous precursor materials into a dense structure within a strongly alkaline environment. As a result of the geopolymerization process, an amorphous gel with binding properties is formed, leading to the creation of an amorphous alumina silicate gel that possesses a compact structure [27].

The chemical process of geopolymerization involves a series of steps:
alkaline activation: Alkaline activation, an intriguing process, utilizes a special alkaline activator to aid in dissolving aluminum (Al) and silicon (Si) from the inorganic precursor. This activator acts as a catalyst, encouraging the condensation reaction to take place. When alumino-silicate oxides (Si_2O_5, Al_2O_2) are combined with a potent alkaline solution, the Si-O-Si bonds undergo disruption, and the aluminum (Al) atoms become integrated into the initial Si-O-Si structure. In the captivating world of geopolymer chemistry, the formation of geopolymer precursors occurs through the creation of alumino-silicate oxide gels. These gels are composed of Si-O-Al blocks and serve as the foundation for the polycondensation reaction. The enthralling dissolution and hydrolysis reaction associated with this process is presented in Figure 2.1.

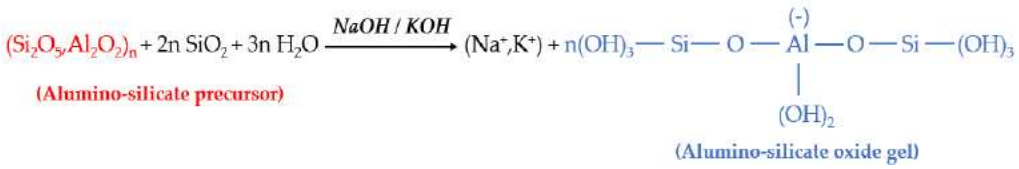

Figure 2.1. Schematic illustration of the formation of geopolymer monomers [28][29].

In the geopolymer network, polycondensation occurs, where the highly reactive alumino-silicate gel swiftly reacts in alkaline conditions, leading to the formation of a robust three-dimensional (3D) framework composed of Si-O-Al bonds. In order to achieve the desired mechanical strength and complete the geopolymerization process, the material must undergo heat curing within a temperature range of 25 to 90 °C. During the polycondensation process, the water generated is typically consumed as part of the dissolution process.

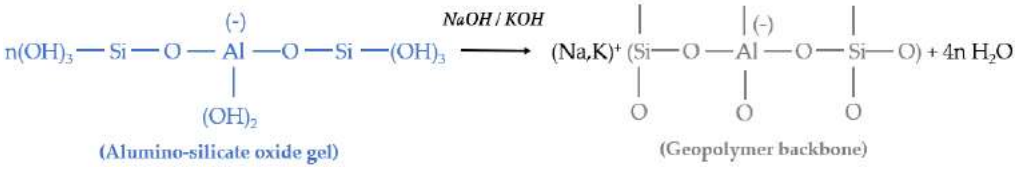

Figure 2.2. Illustration depicting the Polymerization schematic for geopolymer [28].

Polysialate structures constitute the geopolymer networks, where the term "sialate" denotes a building block consisting of Si-O-Al. The presence and arrangement of Si and Al atoms has a crucial impact in determining the ultimate network structure and degree of crystallinity in geopolymer binders. The ratio of Si to Al atoms influences the formation of three distinct silicon-oxo-aluminate tetrahedral structures: (Si-O-Al-O)-type polysialate, (Si-O-Al-O-Si-O)-type polysialate-siloxo, and (Si-O-Al-O-Si-O-Si-O)-type polysialate disiloxo. The specific structure that emerges depends on this ratio.

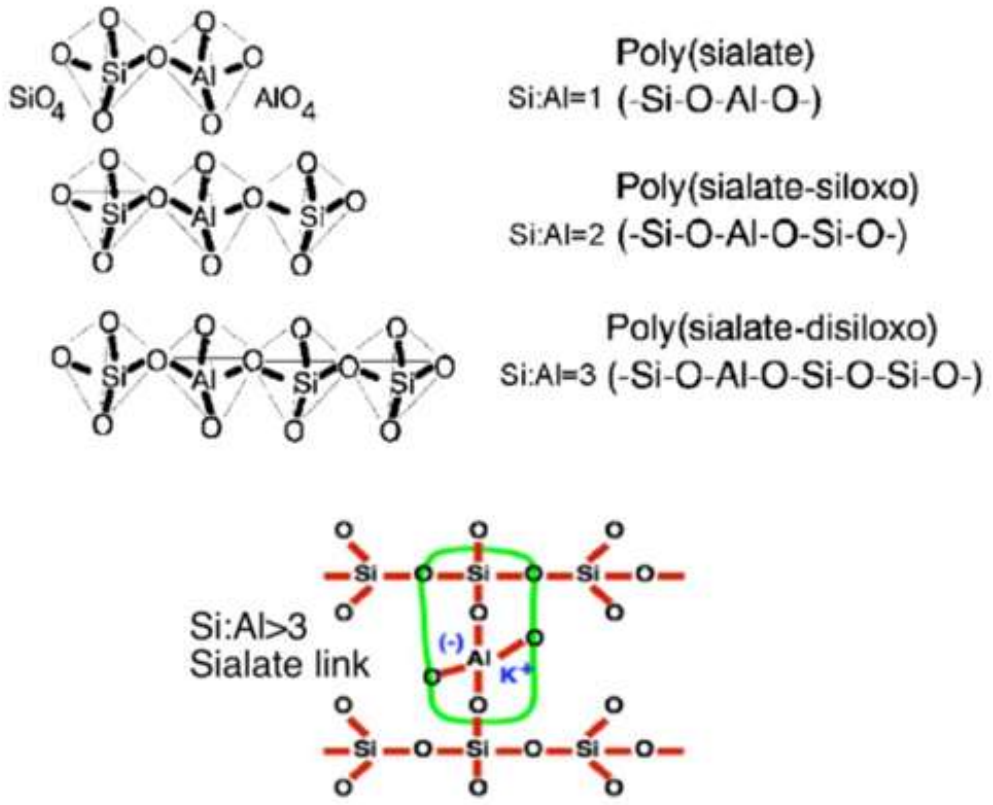

Figure 2.3. Structure of geopolymer [30].

The original model of hydrated sodium aluminosilicate gel formation was later revised by several researchers [31][32][33][34]. According to this revised model, depicted in Figure 2.4, the gel formation entails a series of sequential stages. The process commences with the introduction of aluminosilicate powder precursors into an alkaline activator solution leading to subsequent reactions, causing the aluminosilicates to break down into silicate and aluminate monomers.

During the initial stage of the process, the monomers generated interact with one another, resulting in the formation of dimers. Furthermore, through intermolecular interactions, these monomers engage with other monomers, resulting in the generation of tetramers, trimers, and subsequent complex molecular structures. Once the solution reaches saturation, the process of formation N-A-S-H gel through production. That initial object, identified as "Gel 1," exhibits a significant aluminum content and is regarded as a transient intermediate reaction product [35].

The presence of a concentrated alkaline environment during the primer phases of the reacticity process causes to the shaping of "Gel 1" due to the abundance of Al^{3+} ions. The relatively weaker Al-O bonds, in contrast to the Si-O bonds, expedite the dissolution process of reactive aluminates by allowing for their more rapid dissolution. As the reaction proceeds, a rise in the concentration of silicate is observed in both the reaction solution and the N-A-S-H gel (Gel 2) as a result of the increasing dissolution of Si-O groups derived from the aluminosilicate source. This process influences the pore microstructure, the distribution of voids within the polymer, and the binding capacity of the polymer.

Based on the results of previous studies have presented a simplified version of the geopolymerization process and reaction mechanism. This representation, shown in Figure. 2.4, illustrates that the reaction mechanism is made up of several reactions happening simultaneously, such as dissolution, reorganization, and hardening. It is a summary of the previous studies.

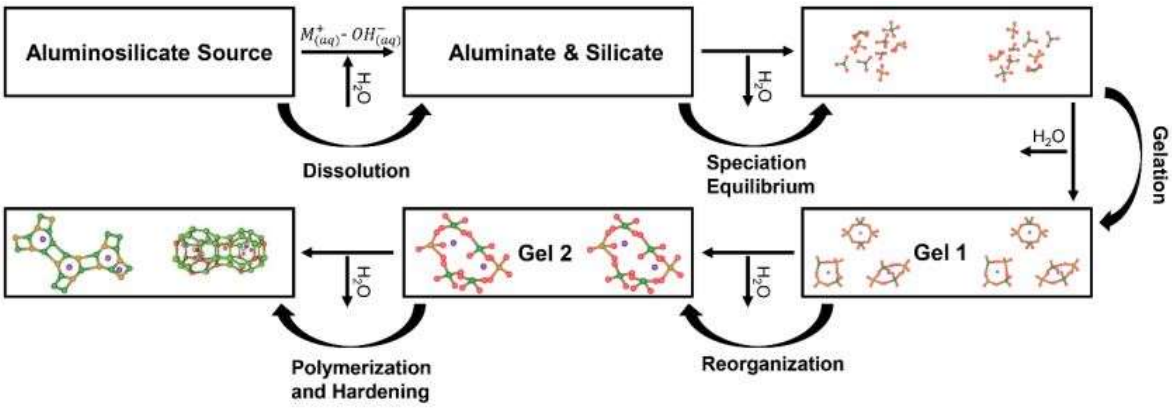

Figure 2.4. Model of geopolymerization processing [36][37].

Provis and Bernal [38] recently proved that the hypothesized process does not apply to calcium-rich alkali-activated systems, such as alkali-activated slag. In response, Provis and Bernal [39] proposed an extended conceptual map of geopolymerization, adapted particularly for calcium-rich alkali-activated systems. This diagram is visually represented in Figure 2.5 for better understanding and clarity.

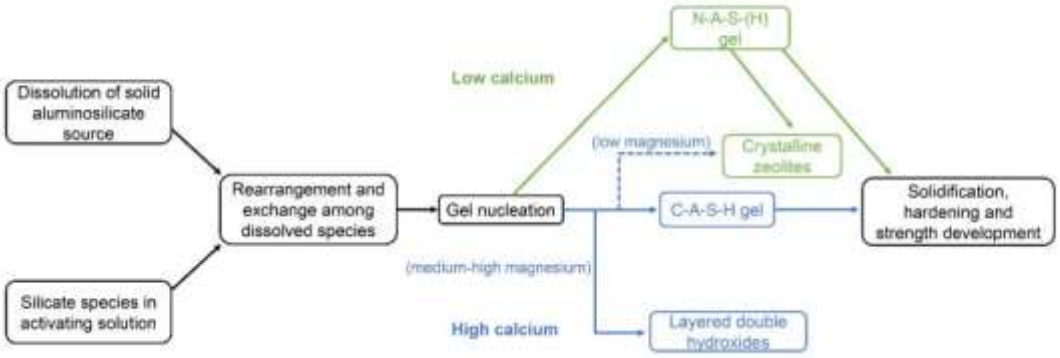

Figure 2.5. Model of geopolymerization for alkali-activated system [39].

This poses a challenge in terms of sourcing suitable precursors for the production of geopolymers in certain regions. Given these challenges, it is essential to explore alternative source materials (precursors) that can be used in geopolymer production to make it more accessible and widely applicable. The research of aluminosilicate precursors that are not in high demand within the cement and concrete manufacturing sectors has recently attracted increasing interest [40]. The goal is to find alternative precursors that are more readily available, cost-effective, and environmentally friendly.

As cities continue to grow and urban transformation projects are undertaken, the generation of CDWs increases. The end of a structure life cycle and the need for new construction also contribute to the generation of CDW. Additionally, natural disasters can also result in a significant amount of CDW. These factors all contribute to the growing problem of CDW management, making it increasingly important to find sustainable solutions for its disposal and use. The management of large quantities of CDW is a global concern. One of the most common ways to deal with CDW is to store and landfill it, but this strategy is expensive and not sustainable in terms of welfare, the economy, or ecology [41]. The capacity of numerous nations to effectively manage CDW is restricted and often rely on outdated methodologies like crushing directly and utilizing it as road base/sub-base filling. The disposal of CDW in this manner can be costly and also environmentally damaging, thus it's important to find more sustainable solutions for the management of CDW. The need for new and efficient methods of

managing CDW is particularly pressing for developing and economically struggling countries. One possible solution is to utilize materials produced from CDWs to generate geopolymeric composites. CDW is a worldwide issue present in numerous regions across the globe. Utilizing components generated from CDW materials such as concrete, tiles, ceramics, bricks, and glass as aluminosilicate precursors in the production of geopolymer binders, along with different-size aggregates, has the potential to drive more impactful and creative control of waste management, as well as the enhanced valorization of higher quality materials. These materials can also be used as secondary raw materials in construction industry applications. Using CDW-based materials to produce geopolymers can be a beneficial solution for managing CDW, particularly in developing and economically struggling countries. By using CDW-based components such as ceramics, concrete, bricks, tiles, and glass as aluminosilicate precursors in the production of geopolymer binders, it has the potential to decrease the quantity of CDW disposed of in designated storage areas and lessen the demand for new production of concrete, precast materials, and aggregates. Although there are studies in current literature that focus on the development of geopolymers using CDW-based precursor materials, they are not as common as studies using more mainstream aluminosilicates.

Ahmari et al. [42] used an alkali activation procedure using NaOH and sodium silicate to create geopolymeric binders including both concrete waste (C) and fly ash (FA). The samples were allowed to sit at the temperature of the room for 24 hours before being taken from their molds and stored in plastic bags for another 6 days. The findings demonstrated that increasing the NaOH solution proportion affected the mechanical enhancement of geopolymeric binder throughout the compressive testing. They also discovered that the inclusion of sodium silicate aided in the development of compressive strength. Furthermore, it was discovered that increasing the percentage of concrete waste up to a specific threshold enhanced geopolymeric binders' compressive strength. The specimens composed solely of C exhibited a compressive strength of roughly 11 MPa following cure at room temperature for 7-day, according to the study. The compressive strength has recorded as about 35 MPa which was the the highest value of it. This was obtained in specimens made up of 50% FA and 50% C, activated by using alkaline solution of NaOH with 10M and sodium silicate with a mass ratio of 2.00.

A series of tests were carried out by Nematollahi et al. [43] on 3D-printed geopolymers fabricated from FA and GBFS materials. The specimens underwent compressive strength tests along three distinct axes, flexural tests along two separate axes, and time-dependent assessments of interlayer bond strength. The latter involved evaluating bond strength at two different time intervals (2 minutes and 15 minutes) following the initial layer's printing. These comprehensive tests were performed by the researchers to assess various mechanical properties of the specimens. The outcomes of the compression tests revealed a significant disparity in strength between the specimens loaded in parallel with the printing direction and those loaded laterally. Notably, the specimens subjected to loading parallel to the printing direction displayed an impressive 72% increase in strength compared to their laterally loaded counterparts. In contrast, in flexural strength tests, only 65% of the lateral loading strength was achieved when loaded perpendicularly to the printing direction. Furthermore, the study reported a maximum strength result of 1.3 MPa in the time-dependent interlayer bond strength test. The objective of this test was to examine the influence of various time delays (2 and 15 minutes) after printing the first layer on the bond strength between two consecutive layers.

Khater [44] applied different methods of curing were applied to the created samples, including curing in water at room temperature and at 40°C with 100% humidity. Some of the samples were tested for compressive strength immediately after curing, while others for 24 hours were dried at 80°C before testing. The study found that mixtures with SiO_2/Al_2O_3 ratios between 3 and 3.8 mechanical properties showed improved. Furthermore, curing immersed in water room temperature was shown to have superior microstructural and mechanical qualities than curing at 40 °C and 100% RH.

In 2016, the viability of producing geopolymeric pastes using CDWs and industrial waste was examined by Zaharaki, Galetakis, and Komnitsas [45]. Aluminosilicate precursors such as red mud, waste brick, electric arc furnace slag (EAFS), waste from tile, and concrete were utilized, along with alkaline activators including solution of NaOH as alkali activator and liquidified form of sodium silicate. They used the precursors individually, in mixtures (up to 50% EAFS replaced with red mud), and in quaternary mixtures (up to 75% EAFS replaced with tile, brick, and concrete mixes). They determined that the proper SiO_2/CaO and

SiO_2/Al_2O_3 ratios, in addition to an appropriate concentration of NaOH, were critical to attaining the desired properties in the final product. In this study, the CDW-containing mixtures achieved a maximum compressive strength of 76 MPa.

The goal of Li et al.'s [46] study was to improve the mechanical qualities of geopolymer mortars made using GBFS and FA. Through the use of continuous micro cable steel, they succeeded. Silica fume was added to the combinations to enhance their thixotropic and microstructural properties in order to make them more suitable for 3D printing. Alkali activation was achieved by including solid penta sodium metasilicate in the dry mixtures. By using experiments like tensile, compression and shear loads, the researchers assessed the 3D printed geopolymers' composite behavior. The findings revealed impressive results, with the maximum 28-day compressive strength recorded as 41.5 MPa, tensile strength as 4.69 MPa, and bond strength as 4.79 MPa.

Chougan et al. [47] investigated the characteristics of sodium silicate (Na_2SiO_3) and NaOH activated geopolymer binders produced from FA, GBFS, and SF for 3D printing. The rheology, mechanical characteristics and buildability of the 3D printed mixes were investigated. Researchers also looked at the impacts of integrating nano-graphite platelets. According to the study's findings, the flexural strength of the 3D printed mixes with 1% nano-graphite platelets increased by 90% when compared to the samples without any of these platelets. Additionally, the compressive strength of the 3D printed samples with nano-graphite platelets was 30% higher. The maximum flexural strength was 15.3 MPa, whereas the highest compressive strength was 50.9 MPa. These findings indicate that the addition of nano-graphite platelets enhances the mechanical properties of 3D printed geopolymer binders.

Muthukrishnan et al. [48] investigated geopolymer concrete made from FA, GBFS, fine and coarse aggregates, magnesium alumina silicate, Na_2SiO_3, and water. To evaluate the mechanical characteristics of the concrete, compressive and flexural tests were done in three distinct directions. The researchers also looked at how alkaline reactions affect the rheological characteristics of geopolymer concrete compositions suited for 3D printing. The researchers examined the impact of several design factors on the rheological characteristics of concrete,

including the activator concentration, the retarder (sucrose), and the dose of the thixotropic additive. The rheological characteristics were tested using a Viskomat XL. Throughout the experiment, a fixed mixer with six blades rotated the outer cylinder to apply a shear force to the material, and the time-dependent change of the applied torque was measured. Shear stress, viscosity, and shear rate were calculated using the Reiner-Riwlin equation, which was enlarged to take torque and rotations per minute (rpm) into consideration. For the duration of the testing period, 3D-printed geopolymer samples were submerged in water to examine their mechanical properties. The results of the test after 28 days showed that the parallel-loaded samples had flexural strength that was 56% higher and compressive strength that was 28% higher than the perpendicular-loaded samples.

Ma et al. [49] utilized Portland cement and FA to produce mortars in a multi-layered form through 3D printing. Three distinct loading directions were used to assess the samples' compressive and bending properties, and the resultant strength data were compared to those of the casted specimens. Additionally, splitting tensile tests were conducted. The study revealed that the samples subjected to compression exhibited a reduction of 7% and 24.6% under perpendicular and lateral loading, respectively, compared to the casted specimens. When loaded in a direction parallel to the printing route, the outcomes were comparable. In terms of flexural strengths, the samples that were parallel and perpendicular to the printing direction illustrated approximately 56% and 20% stronger strength than the casted specimens, respectively. On the other hand, samples that were subjected to side loading had a 24.8% lower strength.

2.2 Construction Industry Automated Fabrication/AM

2.2.1 The historical background of AM Technology

AM technology, or Additive manufacturing technology, is associated with the action of creating physical objects from digital designs using a variety of techniques, such as 3D printing. The history of AM technology can be traced back to the 1980s, when the first patent for a 3D printing process was filed. However, the technology was still in its infancy at that time and was not widely used. It was not until the 1990s that AM technology began to gain traction, thanks to the development of more advanced 3D printing machines and materials.

This decade saw the introduction of several key technologies, such as stereolithography (SLA) and fused deposition modeling (FDM), which are still widely used today. Additionally, the cost of 3D printers began to decrease, making them more accessible to consumers and small businesses [51][52].

In the 2000s, AM technology continued to evolve and expand. Materials such as metal and ceramics were added to the list of materials that could be used in 3D printing, and the technology began to be used in a wide range of industries, from aerospace to healthcare. The introduction of open-source 3D printing software also allowed for greater collaboration and innovation in the field. In recent times, there has been a remarkable surge in the adoption and utilization of AM technology, driven by the development of new materials, improved printing speeds and precision, and the increasing use of the technology in industries such as manufacturing, aerospace, and healthcare. Today, it is estimated that the global market for AM technology will reach $35 billion by 2025, with continued growth expected in the future [53][54].

Some benefits of AM technology can be listed as:

- Customization: AM technology allows for the creation of highly customized and complex parts and products.
- Speed and Efficiency: AM technology can be faster and more efficient than traditional manufacturing methods, leading to significant cost savings and faster time-to-market.
- Reduced Waste: AM technology generates less waste compared to traditional manufacturing methods.
- Cost-effective: As the technology advances, the cost of 3D printing materials and machines is decreasing, making it more accessible to small and medium-sized businesses.
- Accessibility: AM technology is making it easier for people in remote or under-developed areas to produce goods.
- Complex Geometries: AM technology makes it feasible to create complicated geometries and interior structures that would be challenging or impossible to construct using conventional manufacturing processes.

- Reduced tooling costs: AM technology can eliminate the need for expensive tooling such as molds, dies, and jigs.
- Prototyping: Functional prototypes can be made quickly thanks to additive manufacturing (AM) technology.
- On-demand production: AM technology allows for the production of parts on-demand, reducing the need for large inventory.
- Lightweight and strong: AM technology makes it possible to create lightweight and strong parts that can be used in aerospace and automotive industries.
- Design freedom: AM technology allows for greater design freedom, creating complex shapes, and internal structure that can't be manufactured with traditional methods.
- Material versatility: AM technology enables the utilization of diverse materials, such as plastics, metals, ceramics, and bio-materials.
- Personalization: AM technology allows for personalized products, from hearing aids to dental implants.
- Supporting sustainability: AM technology supports sustainability by reducing material waste and energy consumption during production.

As per the ASTM F2792-10 standard [55], AM is characterized as the process of fabricating a physical object by incrementally adding layers of material in a sequential manner. Recently, AM has found widespread application in various industries, including commercial aviation and medical sectors. In the construction industry, AM has been seen as a potential solution to reduce environmental impact, improve product quality, and accelerate building projects [56][57]. The use of AM in concrete production, known as 3D-AM, reduces the requirement for formwork, resulting in considerable cost savings for building projects. Studies have shown that using 3D-AM technology can save construction expenditures by 35-60% compared to traditional methods [58][59]. Furthermore, the utilization of 3D-AM technology, which is supported by advanced equipment, can significantly reduce labor requirements and decrease the risk of accidents. This results in a reduction of both labor costs and accidents [60][61]. Additionally, the use of 3D-AM allows for more flexibility in design, as designers are no longer limited by traditional constraints and can create designs that are both aesthetically pleasing and functional.

Utilizing 3D-AM technology in building has several benefits, including it allows for faster and more consistent production speed. Buswell et al.[62] evaluated completion times for walls built using 3D-AM and conventional techniques and discovered that the walls produced using 3D-AM technology were accomplished at a consistent pace and within a reduced timeframe. Additionally, it was noticed that the walls produced by traditional methods required time for curing, which was not necessary for walls produced using 3D-AM technology.

As technology continues to advance, people have begun to anticipate more from design tools and the possibilities they offer. With the fast-paced, mobile lifestyles of today, there is a need for solutions that keep up with digital technologies. One such solution is 3D printing, which utilizes digital fabrication to produce complex shapes and structures by converting digital models into a series of parallel horizontal slices. This method offers benefits such as quicker construction, cost efficiency, and safe working conditions. 3D printing may come with certain challenges, but it opens up new possibilities for customizable, flexible, and modular housing. Additionally, With the use of this technology, architects are able to design buildings with distinctive and sophisticated geometries that would be challenging or impossible to build using conventional manual construction techniques. This gives designers more creative flexibility.

The primary issue with 3D-AM is creating materials that are suitable for use in the process. To ensure seamless printing without system clogging or instability in the printed elements, these materials require specific properties in both their fresh and hardened states. Moreover, the chosen materials should be easily extrudable, allowing smooth movement from the storage container to the printer hose and nozzle [63]. The materials used in 3D-AM should have the ability to retain their shape, known as buildability, to prevent deformation or collapse under the weight of consecutive layers [64]. Additionally, the printed layers must quickly attain sufficient strength to protect layers from collapsing and maintain structural integrity. This can be achieved by utilizing thixotropic properties in the printed materials, where the viscosity is reduced due to agitation during pumping, allowing the material to be transferred smoothly to the nozzle without issue [65]. Upon the completion of the agitation process, commonly referred to as extrusion, a noticeable augmentation in yield stress and viscosity becomes

evident within the extruded material. This leads to uniformity in terms of the stability of shape and the quality of the surface throughout the layer [63][66]. The materials should also have a sufficient open time, which ensures that there is enough time to maintain the material's buildability and extrudability within an acceptable tolerance range [63][66]. However, if the printed materials harden too quickly (shorter open time), it can negatively impact the extrudability, buildability, and the ability to transfer the materials via an enclosed mechanism, like 3D printing machinery.

In addition to the aforementioned critical features, the printed structures must also have appropriate mechanical performance. The sequential nature of 3D-AM brings forth the potential influence of load orientation and bonding surface among successive layers on the mechanical characteristic of printed structures. Consequently, when designing materials for 3D-AM, it is crucial to consider mechanical characteristics of 3D-printed structures under diverse loading orientations, as well as the bonding strength between adjacent layers as essential factors. To guarantee that the combination is suitable for 3D printing in its hardened condition, changes in the mechanical characteristics of the printed structures should be reduced with respect to the direction of loading. Moreover, it is imperative to ensure a flawless interface region between consecutive layers and to establish adequate binding strength between these layers [67]. Furthermore, during the enhancement of equipment for 3D manufacturing processing, careful consideration should be given to the physical, chemical, rheological and mechanical characteristics of the materials involved. This includes meeting specific requirements in terms of their fresh and hardened states, such as extrudability, green strength, open time, buildability, and bonding. By addressing these factors, the aim is to achieve efficient and effective 3D printing processes. To achieve, compaction (densification), uniform distribution and strong bonding between layers, as well as to produce high-quality end products, it is necessary to design the printing materials and additive manufacturing equipment in parallel.

2.2.2. Reinforcement in 3D-Printing with Fiber Inclusion.

This thesis explores the merging of geopolymers' advantages in material composition and the advanced materials processing approach of 3D-AM, as explored in various recent research. Below, we will delve deeper into the studies pertaining to this subject matter.

In a thorough investigation of Quatifi et al [68] that undertook an extensive investigation that aimed to comprehensively analyze the printability and characteristics of 3D-printed fly ash (FA)-based geopolymers in their solidified state. The geopolymer composition comprised the activation of 0-3 mm sand using NaOH and Na_2SiO_3 as the activators, with a NaOH/Na_2SiO_3 weight ratio of 1. In order to assess the influence of steel and PP fibers on the geopolymer mixtures, three distinct compositions were formulated: one devoid of fibers, another incorporating 0.50% PP fiber, and a third including 1.00% steel fiber by weight. After printing, the samples consisting of three layers of geopolymer mortars were stored for 48 hours at room temperature. Subsequently, a 2-hour heat treatment at 70°C was administered, followed by a 10-day period at ambient temperature for mechanical property testing to be performed. Moreover, the study examined the impact of different time intervals (5 minutes, 10 minutes, and 15 minutes) between the layering process on the mechanical properties of the mixtures. The findings of the study demonstrated a negative correlation between the time interval between layers and the flexural strength of the printed specimens. Intriguingly, it was observed that increasing the time interval led to enhanced buildability performance, as the layers exhibited improved load-bearing capacity, effectively supporting their own weight. In relation to the utilization of steel fibers in AM technology, the study drew the conclusion that their use is not advisable, primarily due to the possible occurrence of surface irregularities between the printed layers

In their research, Nematollahi et al [69] undertook a study to explore the impact of PP fibers on the characteristics of both freshly made and hardened FA-based geopolymer mortars on 3D printed mechanism. The investigation encompassed an assessment of the compressive strengths along three different loading directions, flexural strengths along two distinct loading directions, and an evaluation of the workability and extrudability of the geopolymer mortars. This comprehensive study delved into multiple mechanical properties and performance aspects of the mortars. The findings demonstrated a beneficial influence of incorporating PP fibers on

the compressive strength of the samples when subjected to perpendicular loading, i.e., loading direction perpendicular to the printing path. However, this improvement was not observed in the samples tested under the lateral loading direction. From the compressive strength tests conducted across various loading directions, it was observed that the perpendicular loading exhibited a maximum difference of 20.8 MPa compared to the lateral loading. This difference accounted for 154% of the compressive strength recorded in the lateral loading direction. This implies that the inclusion of PP fibers increased compressive strength substantially when the load was applied perpendicular to the printing path.

A study conducted by Nametollahi et al [70] to investigate how various types of fibers influenced the flexural strength and bond strength of 3D printed geopolymers. The study examined the effects of three fiber types, namely polyvinyl alcohol (PVA), polypropylene (PP) and polyphenylene benzobisoxazole (PBO), in FA-based geopolymer mixtures activated using Na_2SiO_3 and NaOH, and the ratio they have used is 2.5 for Na_2SiO_3/NaOH. The samples underwent tests to assess their flexural strength and interlayer bond strength. The findings revealed that the samples containing added PP, PVA, and PBO fibers demonstrated flexural strengths that were 17%, 23%, and 34% higher, respectively, in comparison to the samples without any fiber inclusion. This improvement was assigned to the ability of the short fibers to bridge cracks, thereby enhancing the flexural strength. Out of the different fiber types, the samples with PBO addition exhibited the highest flexural strength, achieving a value of 10.3 MPa. However, when it came to interlayer bond strength, the results were different. Contrary to what was found for flexural strength, the interlayer bond strength was lower in the samples with fiber added. Compared to the samples without fiber, the inclusion of PVA, PP, and PBO fibers resulted in interlayer bond strengths that were 15%, 20%, and 23% lower, respectively. The variation was attributed to the enhanced rigidity of the mixtures with added fibers, impeding the formation of a seamless bond during the printing process and thereby impacting the interlayer bonding mechanism.

On specimens made of class F FA-based geopolymers, Nematollahi [71] carried out compression tests along three different axes and flexural tests along two different axes. They also looked at the samples' interlayer bond strength. The 8M NaOH solution was mixed with Na_2SiO_3 alkali activators in a 2.5:1 Na_2SiO_3/NaOH ratio to produce the geopolymer mortars.

PVA, PP, and PBO fibers with lengths of 6 mm were also added to the geopolymer mixes separately. Following a 24-hour thermal cure at 60°C, the samples were kept at ambient temperatures until the testing day. The samples' compressive strength at parallel loading is shown to be 50% more than that during lateral loading, as observed from the compression test results. Regarding flexural strengths, when compared to the sample under perpendicular stress, the sample under lateral loading showed a 6.5% increase in strength. The interlayer bond strength, according to the research, varied between 2.33 MPa and 3.03 MPa.

The bending behavior of printed PC mortars made by adding polyethylene fiber in specific proportions were conducted by Ding et al [72]. In all three loading directions, bending tests were conducted on multilayered, extracted, and printed samples, and the outcomes was made a difference to mold-cast samples. At the end of the trial, 50.7% was the value reported as the largest variation in flexural strength in various directions.

The existing research on 3D-AM recognizes that the discrepancies in mechanical performance under various loading directions are influenced by the anisotropic characteristics of the printed materials. These attributes stem from the inherent weak bond regions between layers in the printing process. although, there are still no agreement on how the anisotropic influence emerges on other loading directions, such as perpendicular, parallel and lateral orientations. Moreover, a significant gap exists in this literature, as there are not any research on specifically addressing the anisotropic behavior of 3D printable geopolymers exclusively composed of CDW materials. This emphasizes the need for further research in this promising area of study.

In a comprehensive investigation by Ma et al. [73], a geopolymer composite was studied, consisting of GBFS, FA, SF, silica sand, and ordinary water. In order to reduce shrinkage and water loss, Hydroxyethyl Cellulose and PP fiber were added to the mixture. This resulted in a noteworthy compressive strength of 40.5 MPa in the casted geopolymer specimen. Additionally, the tensile strength of 2.84 MPa was also observed. The study revealed the positive impact of incorporating micro-cables, as combinations with these additives exhibited exceptional printability and a dramatic enhancement in flexural strength for 3D-printed

geopolymer structures. These findings suggest promising applications in advanced structural engineering.

The adhesive strength of a building component manufactured using the 3D-AM process is critical in defining the mechanical properties of the material. Only a few studies that particularly analyze the binding strength of materials made with 3D-AM have been reported in the scientific literature.

Panda, Ting, et al. [74] conducted a comparative investigation utilizing two distinct binding agents to evaluate the flow characteristics and mechanical properties of 3D-printed systems. The study focused on developing cementitious mixtures incorporating OPC and recycled glass aggregate, alongside geopolymer mixtures based on FA. To assess the rheological behavior of the mixtures, various tests were performed, including viscosity restoration, slump assessment, and visual examination. Additionally, casted cubes and 3D-printed specimens were prepared using both binding systems, and compressive strength tests was done carefully on the specimens after 7 days. The findings showed that the OPC-based mixtures exhibited superior thixotropic characteristics compared to the FA-based geopolymer mixtures. Furthermore, In both casted and 3D-printed specimens the OPC-based mixes had a much greater compressive strength. After 7 days, the 3D-printed OPC samples achieved an impressive maximum compressive strength of 23.1 MPa.

Tay et al. [75] investigated how time intervals affected the printed layers using rheological analysis and visual examination., aiming to gain a better comprehend of the material behavior of freshly formed additive layers. On the 28th day after printing, the tensile bond strength among the adjacent to layers of the printed samples were evaluated. The printed samples made at 1-minute intervals had interlayer bond strengths ranging from 0.8 to 1 MPa.

Panda et al. [76] conducted an investigation focused on assessing the adhesive capacity of geopolymer samples derived from 3D printing using FA and GBFS, supplemented with microsilica and activated with NaOH and Na2SiO3. Based on the results of bond strength tests performed at various molar ratios, it was discovered that as the molar ratio fell, there is a

reduction on bond strength due to a decrease in setting time. At the culmination of the research, the highest bond strength recorded among the various MR combinations was 0.734 MPa.

Another research focused on the development and examination of wood fiber reinforced geopolymer composites (WFRGC) using varying amounts of wood fiber (5-35 wt%). The inclusion of wood fibers resulted in a decline in mechanical properties, as evidenced by compressive strength, force load, flexural strength, compressive modulus, and flexural modulus measurements. The study suggests that WFRGC containing 20-35 wt% wood fibers exhibits promise as an environmentally friendly construction material [78].

Another study offers that potential use of steel fibers as reinforcement holds promise, but the effect of the printing process on fiber orientation is still uncertain. The objective of the study is to statistically analyze the distribution of steel fibers in 3D-printed ultra-high-performance concrete and determine how nozzle size, print speed, and fiber volume fraction influence fiber orientation. Results were contrasted with samples that had been conventionally cast. According to the results, the 3D-printed specimens outperformed the cast ones mechanically. This is because of good fiber alignment [79].

3. MATERIALS AND METHODOLOGY

3.1 Materials

A comprehensive description is given regarding the various elements utilized in the production of geopolymer mixtures in this section. It offers a comprehensive overview of the various components, including CDW, recycled aggregate, alkali activators, and fibers, and thoroughly investigates their usage.

3.1.1. Materials in the Making

3.1.1.1. CDW Materials

Geopolymers were synthesized using various materials derived from building and demolition debris. The materials have been used in this research, consist of roof tiles, concrete waste, hollow bricks, glass waste, and red clay bricks were obtained from demolished structures in Turkey. These materials, namely RT, HB, RCB, CW, GW were sourced from demolished structures in Turkey. For the purpose of obtaining clay-based waste materials to be utilized as precursors, careful selection was made focusing on the roof and wall components of these demolished structures, including RT, HB, and RCB. Moreover, GW, which is a CDW material known for its elevated silica content, was primarily obtained from the windows of demolished buildings. Another waste material, CW, was obtained from both structural and non-structural parts of destroyed structures and also served as a precursor.

To reduce the size of larger or coarse elements present in CDW, they were fragmented into smaller particles and subsequently introduced individually into a jaw crusher for initial crushing (see Figure 3.1). The material then underwent a final grinding process using a ball mill for one hour (see Figure 3.2). Specific details of the materials that were crushed and ground can be found in Figures 3.3. It is worth noting that aggregate containing cement (C) was milled together with the aggregate without requiring any specific procedures, unlike other waste products. After milling, a sieve procedure was employed to distinguish between aggregate and concrete waste (hydrated waste).

Figure 3.1. Jaw crusher.

Figure 3.2. Ball mills in Research: visual compilation.

Figure 3.3. Raw, crushed, and grinding phases of the CDW materials.

To evaluate the characteristics of the precursors, laser-based diffraction and XRF studies was utilized for defining distribution of particle size, oxide compositions respectively, after the milling process. To guarantee the correctness of the findings, a representative sample of every powdered substance was taken from the center of each batch, dried in an oven for a whole night, and then analyzed. A wavelength of 0.1–50 Å was employed for XRF analysis was

selected for laser diffraction. Additionally, the team recorded the specific gravities of the milled CDW-based precursors which can be found at Table 3.1.

According to the XRF data, the primary oxides found in the clay-based CDWs were Al_2O_3 and, SiO_2 and then Fe_2O_3, that are critical for geopolymerization processes. In the realm of precursor compositions, the principal oxide proportions showed remarkable similarities, however it was the intriguing oxide structures of GW and CW that set them apart from the other CDW-based precursors. GW, derived from window glasses, boasted a lavish abundance of CaO (~10%), Na_2O (~14%), and SiO_2 (~67%). On the other hand, CW flaunted a distinct blend, with a notable presence of CaO (~32%), SiO_2 (~32%), and MgO (~5%). These distinctive oxide configurations added an element of fascination to the mix [77][79][82][83].

Table 3.1. Outcome of XRF analysis [81].

Percent (%) of oxides	**HB**	**RCB**	**GW**	**RT**	**CW**
SiO_2	39.7	41.7	66.5	42.6	31.6
Al_2O_3	13.8	17.3	0.9	15.0	4.8
Fe_2O_3	11.8	11.3	0.3	11.6	3.5
CaO	11.6	7.7	10.0	10.7	31.3
MgO	6.5	6.5	3.9	6.3	5.1
Na_2O	1.5	1.2	13.6	1.6	0.45
K_2O	1.6	2.7	0.2	1.6	0.7
SO_3	3.4	1.4	0.2	0.7	0.9
P_2O_5	0.3	0.3	0.0	0.3	0.1
Mn_2O_3	0.2	0.2	0.0	0.2	0.1
Cr_2O_3	0.1	0.1	0.0	0.1	0.1
TiO_2	1.7	1.6	0.1	1.8	0.2
Loss on ignition	7.8	8.0	4.3	7.5	21.1
Specific gravity	2.89	2.81	2.51	2.88	2.68

The CDW-based precursors obtained varied in terms of grain size distributions after continuous grinding for 60 minutes. As shown in Figure 3.4, GW had the coarsest grain size, while RCB and RT had granulometries that were slightly finer than HB. Approximately 90% of the particles in HB, RCB, and RT were coarser than 45 μm. CW had a larger particle size compared to the precursors derived from clay-based materials. GW remained the coarsest, with nearly 70% of its grains coarser than 45 micrometers. The observed variations in the particle size distributions of the substances can be attributed to inherent discrepancies in the characteristics of the raw materials, such as density, pore structure, and other factors. Given the difficulty, expense, and energy-intensive nature of achieving comparable particle size ranges for all CDW-based materials, no further attempts were made to adjust or modify their particle size distributions.

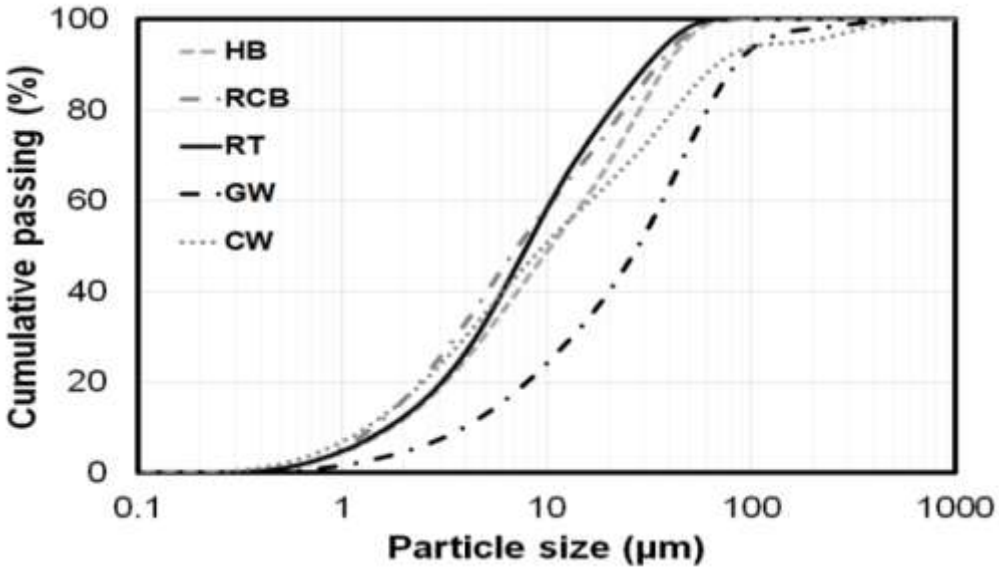

Figure 3.4. The distribution of particle sizes in the precursor materials[84].

Instead of using aggregate sourced from natural materials, the synthesis of the geopolymer mortar mixture utilized coarse recycled concrete aggregate (RCA) derived from concrete debris. To ensure compatibility with the printing application techniques, the maximum size of the aggregate in each mixture was limited to 2.00 mm. The concrete rubble was initially reduced in size using a jaw crusher with a 2.00 mm open-side setting. The resulting crushed RCAs were then sieved using a 2.00-mm sieve. Without implementing any additional

processing methods to enhance the strength and mechanical properties of the RCA, they were directly incorporated into the geopolymer mixes. No further adjustments or modifications were made to the particle size and other characteristics of the RCAs and CDW-based precursors.

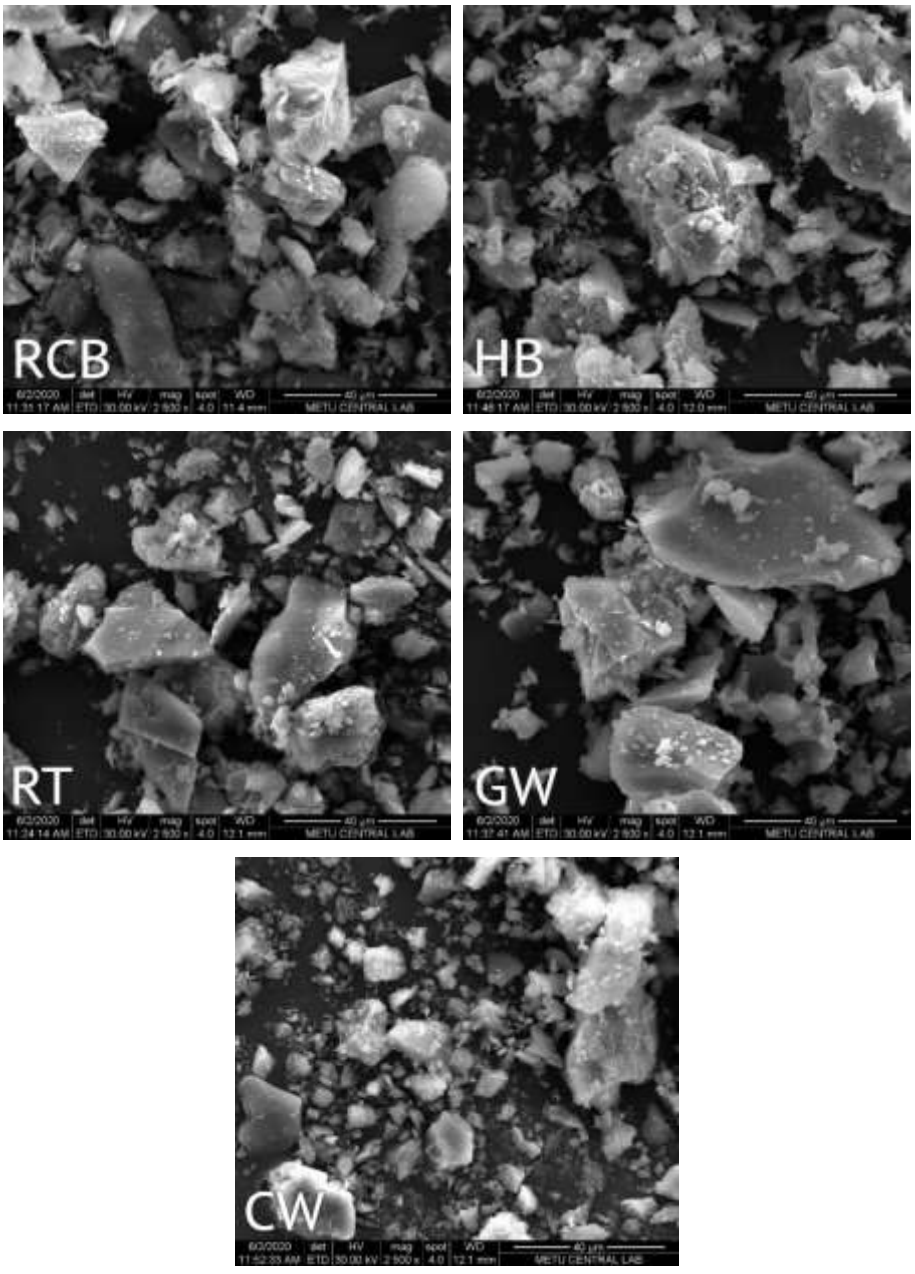

Figure 3.5. CDW-based precursor SEM micrographs [81].

A number of images of the precursors produced using an SEM with a working distance of about 10 mm and a 30 kV voltage under vacuum are shown in Figure 3.5. The SEM micrographs (Figure 3.5) reveal the morphology of the precursors, highlighting the unique angular shape bestowed upon them by the grinding process.

Figure 3.6 illustrates the crystalline phases of the CDW-based precursors, as determined by XRD analysis. The analysis involved scan of the dry samples within the range of 5-55º, with an incremental step of 0.02º. The XRD patterns of the precursors derived from clay (RT, HB, RCB) exhibited a spectrum of phases ranging from amorphous to semi-crystalline in nature.

The observed patterns exhibited similarities to each other, with a broad range of peaks predominantly concentrated around 2θ values of 27-29°. Additionally, different crystalline peaks displayed varying intensities. As anticipated, primary crystalline peak observed in, RT, HB and RCB was the quartz phase, exhibiting the highest intensity. Diopside was identified as another significant peak across all CDW units. Regarding CW, the main peaks identified corresponded to Quartz, Diopside, and Calcite. In contrast, GW exhibited an amorphous nature, as evidenced by a broad peak centered around 2θ values of 28°. Table 3.2 presents the detected crystalline phases for different CDW-based precursors. In the case of CW, the top three peaks corresponded to quartz, diopside, and calcite, while minor peaks were attributed to muscovite and foshagite. Table 3.2 presents an intriguing collection of chemical formulas derived from the XRD analysis of CDW-based precursors. Alongside these formulas, the table includes the corresponding powder diffraction files, providing essential data for the characterization of these materials.

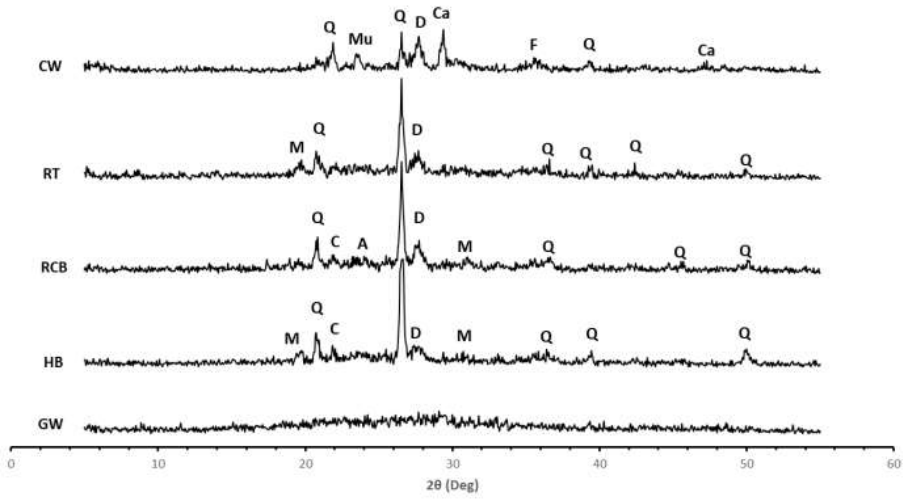

Figure 3.6. XRD models of CDW-based precursors.

Table 3.2. The XRD investigations yielded chemical formulas and assigned Powder Diffraction File (PDF) numbers for the crystalline phases

Symbol	Crystalline Phase	PDF Number	Chemical Formula
A	Akermanite	96-900-6115	$AlCa_2Mg_{0.4}O_7Si_{1.5}$
Q	Quartz	96-101-1160	SiO_2
Ca	Calcite	96-900-9668	$CaCO_3$
Cr	Crystobalite	96-900-8230	SiO_2
D	Diopside	96-900-5280	$Al_{0.6}CaMg_{0.7}O_6Si_{1.7}$
M	Mullite	96-900-5502	$Al2_2O_5Si$
F	Foshagite	96-901-1044	$Ca_4H_2O_{11}Si_3$
Mu	Muscovite	96-101-1050	$Al_3H_2KO_{12}Si_3$

3.1.1.2 Blast Furnace Slag (BFS)

The integration of BFS took place in the blend formulation, whenever it was essential to enhance specific engineering characteristics of the geopolymer combinations. Anticipations suggest that this substance holds the potential to bring about substantial alterations in the behavior of blends and aid in addressing the deficiencies found in mixtures solely comprised of 100% CDW-derived elements. This improvement can be achieved through the enhancement of mechanical and rheological characteristics within the mixtures. BFS, sourced as an

industrial waste, was acquired from the iron-steel plant located in Hatay-Iskenderun Turkey. In Figure 3.7, the overall view of the BFS powder is presented.

Figure 3.7. Blast Furnace Slag Powder.

3.1.2 Alkaline Activators

Based on an extensive literature review and preliminary studies conducted across various projects, the thesis focuses on the utilization of two distinct alkali activators, namely NaOH and $Ca(OH)_2$. These activators are chosen based on their efficacy and findings from prior research endeavors [86][87][88][89][90].

3.1.2.1. Sodium Hydroxide (NaOH)

Caustic soda, alternatively referred to as sodium hydroxide (NaOH), finds extensive application in chemical manufacturing and holds a significant presence in multiple sub-branches. NaOH, which is available in various phases and forms, can be produced through the electrolysis of water and sodium chloride. Solid NaOH is commonly available in the form of flakes, beads, or sticks, all of which have identical chemical compositions. The reaction between NaOH and water leads to the dissociation of NaOH into sodium (Na^+) and hydroxide (OH^-) ions. This reaction is highly exothermic, generating significant heat. The released OH^- ions raise the alkalinity of the environment around them, which raises the pH of the system.

Al and Si minerals in binder materials dissolve more easily as a result of the increased alkalinity. Among various activators, NaOH is extensively employed as the most commonly

used activator in alkali activation research, largely because of its accessibility and affordability. However, as the heat produced during their manufacture can present threats to workplace health and safety, it is necessary to deal with NaOH solutions carefully. As a result, taking the appropriate safety precautions is required when making NaOH solutions. In this investigation, white flake NaOH with a density of 2.12 g/cm^3 was utilized. The NaOH had a minimum purity of 98% and maximum impurities of 0.40% sodium carbonate, 0.10% NaCl, and up to 15 mg/kg iron. Figure 3.8 provides a visual representation of the flake format of NaOH used in this study.

Figure 3.8. Flaked format of NaOH.

3.1.2.2. Calcium Hydroxide

Calcium hydroxide, is a chemical compound that is produced when quicklime reacts with water. $Ca(OH)_2$ is utilized as an activator in the geopolymerization process due to its chemical form, which enhances the alkalinity of the system when dissolved in a medium. This characteristic of $Ca(OH)_2$ has led to its application as an activator in the literature, owing to the benefits it provides to the geopolymerization process. In addition to enhancing alkalinity, calcium hydroxide can accelerate the reaction by serving as an additional source of "Ca" in the structure. This contribution of calcium hydroxide promotes the formation of C-S-H and C-A-S-H structures within the system, leading to the development of a denser matrix formation. The incorporation of $Ca(OH)_2$ is expected to enhance the mechanical properties of the matrix by promoting the formation of a denser structure with increased C-S-H and C-A-S-H structures. To activate geopolymer systems, calcium hydroxide can be introduced directly into

the system in powder form or combined with water for the reaction to take place. The powder form of $Ca(OH)_2$ used in this investigation exhibited specific properties. Figure 3.9 provides an overall depiction of the $Ca(OH)_2$ powder used in the study [88][91][92].

Figure 3.9. Calcium Hydroxide powder.

3.1.3 Recycled Concrete Aggregate (RCA)

Waste aggregates, particularly reinforced structural materials like CW, significantly contribute to the overall portion of CDW. Therefore, it is crucial to ensure proper recycling of these materials. The utilization of recycled aggregates in geopolymer systems provides an excellent possibility for recovery. In this thesis work, recycled aggregates were obtained by sieving crushed-ground CW batches and then integrated into CDW-based geopolymer mortars.

To ensure the smooth operation of the 3D-AM process and avoid blockage or transportation issues, the recycled concrete aggregates (RCA) were limited to a maximum size of approximately 2.00 mm. The limitation considered the constraints on particle size due to the pump model and capacity of the lab-scale 3D-AM system.

To obtain RCA, the CDW-based concrete rubbles were first crushed by utilizing a jaw crusher. Subsequently, the crushed material was sieved through a sieve with a 2.00 mm-opening to separate and collect the desired RCA. The aggregates were used as-is without undergoing any additional treatment or modification to improve their performance. Figure 3.10 presents a visual depiction of the sequential steps involved in this process.

Figure 3.10. From left to right, the raw, crushed, and grinding phases of the RCA.

3.1.4 Fibers

3.1.4.1 Waste Wood Fibers (WWF)

The waste wood fiber (WWF) used in this study were collected from various construction units and demolition sites, with their origin being unknown. Since the characterization of WWF was essential because wooden units and WWFs derived from CDW often contain a mixture of different substances due to the manufacturing process and the varied conditions they encounter during their service life [93].

To prepare the waste wood for further analysis, it underwent a chipping process using an industrial chipping machine. The machine ensured that the wood was chipped into pieces no larger than 2.00 mm in size. Subsequently, the WWFs were obtained by sieving the chipped material through #20 and #10 sieves in a laboratory setting. The sieving procedure yielded wood waste fibers (WWFs) with particle sizes ranging from 0.85 to 2.00 mm. One crucial aspect of the sieving process was to eliminate wood dust particles below 0.85 mm in size, as they have a significantly higher potential for water absorption.

In order to acquire data regarding the physical characteristics of the WWFs, a sample of 100 fibers was chosen randomly and measured. The average length of the WWFs was found to be 12.45 ± 3.53 mm, while the width measured at 1.3 ± 0.23 mm. Additionally, the depth of the WWFs was recorded as 0.5 ± 0.18 mm. These measurements provided insight into the overall

size and shape of the WWFs. Additionally, the aspect ratio of the fibers was determined to be approximately 10, indicating a relatively elongated shape.

3.1.4.2 Polyvinyl Alcohol (PVA) Fiber

PVA fibers, also known as polyvinyl alcohol fibers, are synthetic polymer fibers that have gained considerable attention across various industries and applications. These fibers are derived from the hydrolysis of polyvinyl acetate, resulting in a material with exceptional physical properties. PVA fibers possess high tensile strength, excellent abrasion resistance, and superior chemical stability, rendering them suitable for a wide range of uses. One standout characteristic of PVA fibers is their remarkable water solubility, enabling easy dissolution and removal after use. This property proves particularly advantageous in applications requiring temporary reinforcement, such as in concrete structures. In our study, PVA fibers of lengths 6.00 mm, 8.00 mm, and 12.00 mm were utilized (Figure 3.11). They are conveniently packaged in 20 kg packs, facilitating ease of handling and storage during our experimental investigations. The measured density of these PVA fibers stands at approximately 1300 kg/m^3, contributing to their lightweight nature and potential for weight reduction in various applications. Moreover, the nominal strength of these fibers is an impressive 1600 MPa, attesting to their capacity to withstand significant loads and stresses.

Figure 3.11. Polyvinyl alcohol (PVA) fiber.

3.1.4.3 Polypropylene (PP) Fiber

Polypropylene (PP) fibers are widely recognized as a versatile and commonly used type of polymeric fiber. In this thesis study an examination was conducted on PP fibers measuring 6.00 mm in length (Figure 3.12). These fibers were conveniently available in 25 kg packs, facilitating easy handling and usage in experimental setup. One important characteristic of PP fibers is their relatively low density, which in our case was measured to be approximately 900 kg/m^3. Additionally, the nominal strength of the PP fibers used in our study was determined to be 880 MPa, indicating their ability to withstand substantial loads and stresses. The incorporation of PP fibers in concrete can enhance its mechanical properties and durability. The versatility, mechanical properties, solubility, and compatibility of PP fibers have positioned them as a valuable material in diverse sectors, facilitating advancements in construction.

Figure 3.12. Polypropylene (PP) fiber.

3.2. Methodology

In this section, comprehensive information regarding the experimental procedures employed in the study is presented. This includes details on the preparation of the mixture and specimens, as well as the testing procedures conducted.

3.2.1. Mixture Preparation Process

Initially, water was combined with flake-shaped NaOH particles in a predetermined proportion to create a customized solution for precursor activation. It is worth noting that the dissolution reaction of NaOH generates heat, causing the temperature of the prepared solution to rapidly rise shortly after the reaction commences. In consideration of workplace safety measures, the pre-fabricated solution was carefully maintained at standard temperature to mitigate the increase in temperature. In this phase, a closed bottle was employed to store the solution in order to avoid water evaporation, as it can lead to alterations in solution molarity and the water/binder ratio within the system. The proportions of activators, binder materials, and aggregates utilized in the designed mix were determined based on previous studies conducted by the thesis advisor and relevant literature, ensuring consistency and alignment with established practices. During the initial phase of mix process, powdered materials, involving $Ca(OH)_2$, are combined and blended together in a mixer for a duration of 2 minute to achieve a uniform dispersion of the powdered components. Once the powder materials were evenly distributed, the ready NaOH solution is carefully introduced to the mixer in a gradual manner while the mixer continued to operate. To ensure a consistent dispersion of sodium hydroxide within each powdered component, the mixture underwent an additional minute of mixing at a reduced speed. This step was taken to attain a uniform dispersion of NaOH throughout all the pulverized substances. Following that, the subsequent steps in the mixing procedure varied depending on whether the mixture included fibers or not. In the case of fiber-containing mixtures, the fibers were introduced to the mixer immediately after achieving a uniform dispersion of sodium hydroxide (approximately 1 minute after adding NaOH) (Figure 3.13), and the blend was further stirred for an additional 5 minutes. For mixtures without fibers, after achieving a uniform dispersion of sodium hydroxide, the mixing process continued for an additional two minutes before concluding.

Figure 3.13. Adding WWF– Polypropylene (PP) fiber to mixture.

3.2.2. Specimen Fabrication

3.2.2.1. Mixture Properties

Considering the optimal rheological properties and based on previous studies for 3D printing, geopolymer mixture proportions were determined. The geopolymer mixture (GEO) design consisted of 60.00% materials made primarily from bricks (RT, HB, and RCB), 10.00% GW, 10.00% CW and, 20.00% slag. In order to maintain the extrudability property and avoid issues during the printing process, a lower aggregate/binder ratio is chosen for the mixtures in this thesis, considering the use of fine aggregate. Additionally, water plays a crucial role in the geopolymerization process, establishing a conducive setting for the breakdown of alumina-silicates and aiding the movement of (OH^-) ions. As a chemical component, the water included in the combinations is not actively involved in the geopolymerization process. However, it is critical to providing adequate workability and establishing the crucial liquid medium for Al-Si dissolution. For each combination in this investigation, a ratio of 0.35 between the aggregate and binder, and a water-to-binder ratio (W/B) of 0.33 (based on weight) were chosen. To determine the mechanical properties and impact of various fibers at the developed geopolymer, mixtures were prepared for 3D printing. These mixtures consisted of a combination of 4.00% $Ca(OH)_2$ and 10M NaOH, which were recognized as the optimal combination and dosage for attaining the highest level of performance, based on previous studies [94][95][96].

The use of fibers in the mixtures increases viscosity and reduces flowability, resulting in decreased printability performance. Therefore, the molarity of NaOH was limited to 10M to prevent an increase in viscosity and maintain the desired printability of the mixtures. The $Ca(OH)_2$ content was constrained to 4.00% of the binder's weight. This restriction is crucial as greater quantities of $Ca(OH)_2$ result in elevated geopolymerization byproducts and solid content, leading to diminished flowability and printability capabilities.

Table 3.3 outlines the geopolymer mortar combinations developed in the thesis that exhibited the desired form ability to maintain shape and capacity for extrusion necessary for the 3D-AM technique. These attributes were accomplished without the need for supplementary chemical additives.

Table 3.3. Geopolymer mortar mixture proportions.

Specimen Name	Fiber (g)	CDW-based precursors (g) (1000 g)					RCA (g)	Alkali Activators				Slag	W/B Ratio
								NAOH		CA(OH)2			
		RT	HB	RCB	GW	CW		Molarity (M)	Amount (g)	Rate (%)	Amount (g)		
GEO-Plain	0.00	200	200	200	100	100	350	10	133	4	40	200	0.33
GEO- 0.50% WWF	6.70												
GEO- 2.00% WWF	13.40												
GEO- 4.00% WWF	26.80												
GEO- 6.00% WWF	40.20												
GEO- 0.25% PVA	2.98												
GEO- 0.50% PVA	5.95												
GEO-0.75% PVA	8.92												
GEO-1.00% PVA	11.90												
GEO-0.25% PP	2.25												
GEO-0.50% PP	4.50												
GEO-0.75% PP	6.75												
GEO-1.00% PP	9.00												

3.2.2.2. Casting Process

Upon completion of the mixing process, cubic specimens (Figure 3.14) measuring 50x50x50 mm^3 were readied by pouring the newly prepared mixtures were poured into molds that had been pre-coated with oil, aiming to evaluate the compressive strength of geopolymer mixtures based on CDW. Additionally, cuboid rectangular prism (Figure 3.15) with dimensions of 240x80x15 mm^3 were utilized for measuring flexural strength.

The cubic samples were initially kept inside their molds, while their surfaces were protected by plastic sheets, for a period of 24 hours at a temperature of 25±2 °C. After the initial day, the cubic specimens were taken out of their molds and subjected to the curing process until they reached the specified testing timeframes.

Figure 3.14. 50x50x50 mm^3 empty and poured cubic molds.

Figure 3.15. 240x80x15 mm^3 empty and poured cuboid rectangular prism molds.

3.2.2.3. Three-Dimensional Additive Manufacturing Process

The process of 3D-AM is complex and interrelated, where numerous factors significantly influence the overall excellence of materials that have been printed. The quality of the printed materials is influenced by factors such as the properties of the materials used, shape of the nozzle, the printing speed, and the flow rate. Previous studies have highlighted the significant influence of these elements on the final outcome. However, it is worth mentioning that this thesis study concentrates on specific aspects and does not extensively explore all of these elements. Laboratory-based printing experiments were performed to evaluate the qualities of the mixes generated in this study for 3D printing. The detailed specifications of the 3D printer employed in this thesis study are depicted in the Figure 3.16. Throughout the printing process, a rectangular nozzle with dimensions of 25×18mm was utilized. The optimal printer speed of 60 mm/sec was determined based on the flow rate of the pump, as indicated by the findings of the preliminary experiments [97][98].

Figure 3.16. Specifics on the lab-scale 3D printer.

During the specimen preparation stage, two-ply filaments with a length of 120 cm were printed to evaluate the 3D-AM-specific properties of the geopolymer mortar mixtures. (Figure 3.17 A). Once the printing process was completed, the fresh filaments were carefully cut to the desired dimensions using a spatula that was sharpened for this purpose (Figure 3.17 B). For the purpose of performing test for the strength of bonding between layers, as well as tests to evaluate the compressive and flexural strength with directional dependence, the filaments were divided into cubic specimens (~40×30×30 mm^3) and prismatic specimens (~160×30×30 mm^3). The specimens were placed on the printing table with their surfaces were kept covered for approximately one day covered for about a day to ensure they attained the required stiffness and resistance without collapsing or disintegrating. Then, for additional curing, they were moved to the curing environment.

A **B**

Figure 3.17. The preparation of the specimens involved (A) utilizing two-ply filaments and (B) cutting fresh filaments.

3.2.3 Testing

3.2.3.1 Flexural Strength Testing

Both geopolymer specimens casted and printed were subjected to evaluation to four-points and three-point flexural tests using universal displacement-controlled test equipment. As illustrated in Figure 3.18, the test was conducted in two orientations: one parallel to the printing direction and one perpendicular to the printing direction. The test's goal was to determine the

specimens' anisotropic flexural strengths. The crosshead speed on the test machine was set at 0.005 mm/sec. The purpose of the flexural strength test was to assess the interlayer bonding between two consecutive printed layers. Prior to testing, the dimensions of each specimen were measured to calculate the flexural strength using the formula provided below.

$$\sigma = \frac{M.y}{I} = \frac{3FL}{2bh^2}$$

The equation utilizes various parameters to compute the flexural strength (σ) of the tested specimen. In this equation, y symbolizes the vertical distance perpendicular to the neutral axis, M denotes the moment of the neutral axis, I signify the second moment area of the neutral axis, L represents the length of the specimen, F denotes the maximum force applied, h represents the thickness of the specimen, and b represents the width of the specimen.

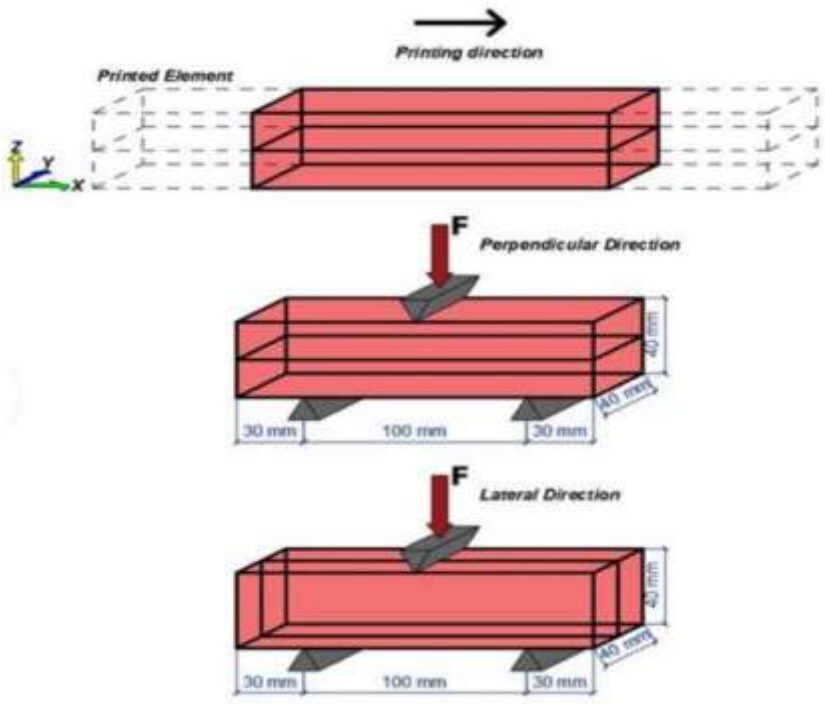

Figure 3.18. General Schematic View Flexural Strength of 3D-Printed Sample [84].

Figure 3.19. Images of prismatic samples under various loading circumstances.

3.2.3.2 Compressive Strength Testing

Two types of samples were subjected to compressive strength testing: casted cubes measuring 50 mm on each side, and printed cubes measuring 40 mm on each side. Following the guidelines of the ASTM C109 (2016) standard, casted specimens (50 mm-cube) and printed specimens (30 mm-cube) were subjected to compressive strength tests utilizing a hydraulic testing machine. The tests were conducted with a loading rate of 0.90 KN/s and a capacity of 150 tons. Due to the varied mechanical reactions generated by the load direction in the process of layer-by-layer fabrication, extensive research is needed to verify the trustworthiness of 3D-printed components. To maintain equal compression areas for each 3D-printed specimens, 30x30 mm steel plates are placed on the surfaces subjected to compression of the specimens. Compressive strength tests on printed cubic specimens for each selected combination were performed to investigate the directional dependence of mechanical properties. These evaluations were conducted in three distinct loading orientations, specifically perpendicular, parallel, and lateral to the direction of printing, as depicted in Figure 3.20. Before testing, the dimensions examined sample were measured to guarantee precise measurements and to eliminate mistakes caused by dimensional changes produced by the printing or cutting procedures. This was done to compute the real regions under compressive load quantitatively. The compressive strength parameters of the printed specimens were derived by dividing the load at failure by the subjected area experiencing compressive forces.

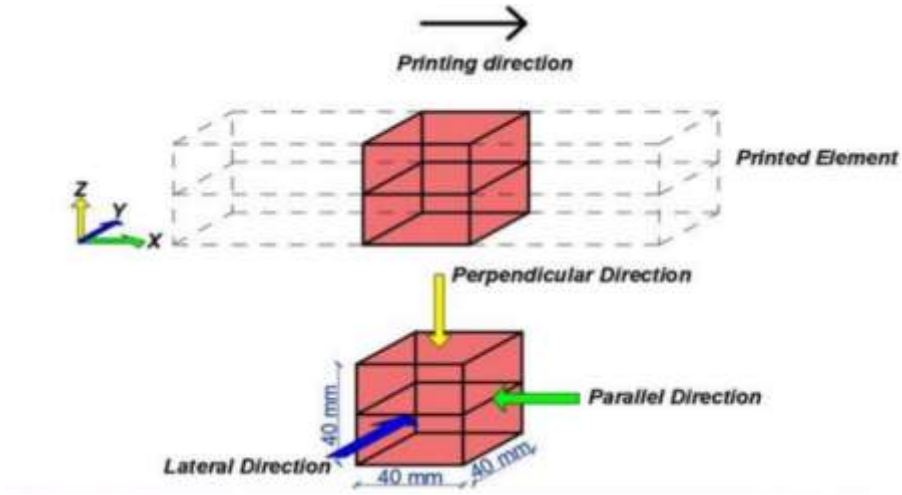

Figure 3.20. General view of printed specimens for 3 types of compressive stress [84].

3.2.3.3 Interlayer Bond Strength

The durability of structures created using 3D-AM technology relies heavily on the strength of the connections between each layer. These connections, also known as interlayer bonds, are relatively fragile because of the unique characteristics of 3D-AM. The weak connection has a vital role in the unequal behavior of 3D-printed items. The current study used direct tensile testing to better understand the bonding mechanism. Interlayer strength of the bond between two successive layers in 3D printing was tested by performing a direct tensile strength test on 40-mm cubic specimens, inspired by Nematollahi et al [99]. The 40-mm printed cubic samples were attached to the T-shaped metal profiles using epoxy-based glue 4 days before testing (Figure 3.21).

Figure 3.21. From left to right, T-shaped metal profile, glued profile, glued sample.

Using a brush, the epoxy was evenly placed across the T-shaped profile as well as the top and lower sections of the sample, maintaining a straight alignment to minimize eccentric loading. To avoid any eccentricity on the testing day, the T-profiles attached to the sample were connected to a metal plate with a single hole with a pintle chain link. Subsequently, the single-hole metal plates were positioned in the tension machine, and the specimen was subjected to direct tensile stress (Figure 3.22). The initial application of the direct tensile strength test was to assess the bonding strength between the printed layers. Following testing, measurements of the bonding zone were collected to properly compute the actual area under strain, preventing errors arising from variations in dimensions. The interlayer bond strength values were determined by dividing the load at failure by the effective area subjected to tension loading, and the strength measurements were averaged across three multiple copies of each sample tested for each specific period of curing at each curing duration.

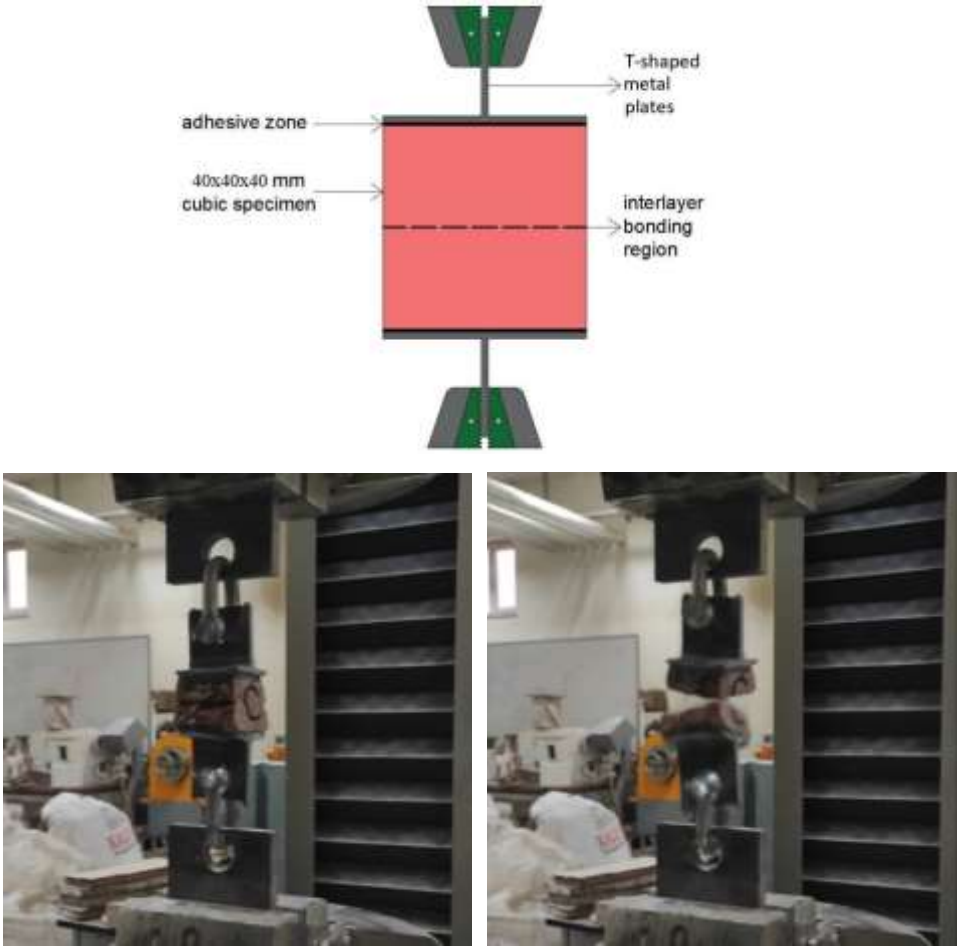

Figure 3.22. Sample subjected to direct tensile stress.

3.2.4 Alkali Treatment Protocol

The initial step in the process involved the treatment of waste wood fibers (WWFs) to remove CDW-based incompatible parts present on their surface, such as paint. To begin with, the WWFs were subjected to a pre-drying stage at a temperature of 50°C. During this pre-drying phase, weight measurements were taken at 3-hour intervals until the weight loss was less than 1.00%. This ensured that the WWFs were adequately dried and ready for further treatment. Once the WWFs were dried, they were then immersed in an alkali solution for a duration of 2 hours. (Figure 3.23) The alkali solution used was prepared by combining flake form NaOH, which had a purity of 98%, with water to create a solution with a molarity of 2.0. The density of the NaOH solution was determined to be 2.13 g/cm^3. The immersion of the dried WWFs in the alkali solution was carried out to facilitate the treatment process.

Figure 3.23. Process of immersing WWFs in an alkali solution.

Figure 3.24 provides a visual representation of the untreated WWF and the WWF treated with alkali. The figures show the color changes that occurred as a result of employing alkali treatment. The untreated WWF exhibited its natural color, while the alkaline-treated WWF displayed a shift in color from brown to dark brown. The alteration in color was ascribed to the elimination of wax oil and lignin from the WWFs, which took place during the alkali treatment process. To ensure the safety and stability of the alkali solution, it was allowed to reach the ambient temperature by keeping it at room condition. This precaution was necessary due to the exothermic nature of the reaction between NaOH and water. Once the alkali solution reached the desired temperature, The pre-dried WWFs were submerged in their

designated solutions at room temperature for the specified treatment durations. This step ensured that the WWFs underwent thorough treatment with the alkali solution. Finally, after the treatment process was complete, the WWFs were rinsed to remove any remaining residue and then dried the specimens were subjected to an oven heat treatment at a temperature of 50°C. This drying stage served to further stabilize the treated WWFs and prepare them for subsequent use or analysis [93].

Figure 3.24. Untreated WWF and the WWF treated with alkali.

4. RESULTS AND DISCUSSION

This section focuses on investigating the impact of various types of fibers, including WWF, PVA, and PP, as well as different fiber lengths and amounts, in 3D-printable geopolymer systems. The investigation involved conducting flexural, tensile, and compressive strength tests to assess the impact of these factors on the resultant mechanical properties. For the achievement of the specified objectives, the utilization of WWF as one of the CDW materials was undertaken. Due to the limitations posed by the chipping process of wood, it became necessary to employ wood with lengths mentioned at section 3.1.4.1, Consequently, a series of casted samples, each containing varying proportions of WWF, were meticulously prepared and rigorously tested. Through a comprehensive evaluation process, the optimum ratio of WWF was successfully identified. The primary aim was to identify the most suitable percentage for the 3D printing process. In contrast to WWF, where the feasibility of selecting different lengths was constrained, the evaluation of synthetic fiber involved the testing of three distinct lengths of PVA within the casted samples. Following the identification of the optimal fiber length, subsequent tests were conducted using different proportions of both PVA and PP fibers to determine the most favorable percentage for the given application. These rigorous experimental procedures were carried out to ascertain the most appropriate combination of materials for enhanced performance and efficiency during the 3D printing process.

4.1 Optimizing WWF Ratios for Casted Geopolymer

To assess the mechanical characteristics of the 7-day-old samples, a thorough analysis was carried out, focusing on the flexural strength-displacement characteristics. These samples were prepared as plain GEO without fiber and GEO, incorporating WWF treated with 2.5M NaOH at, 0.50, 2.00, 4.00 and 6.00 volume percentages. The treatment duration for these samples was set at 2 hours to ensure adequate incorporation of the WWF. The flexural strength-displacement graphs were plotted, revealing insightful findings regarding the performance of the samples. Among the 7-day-old specimens, it was observed that specimens with WWF-inclusion by 0.50, 2.00, 4.00 and 6.00 vol% exhibited 3.68, 3.85, 3.82, 3.05 MPa flexural strength, while displacement values of these specimens were 0.24, 0.28, 0.26, and 0.24 mm, respectively. Notably, the sample containing 2.00% WWF showcased the highest flexural

strength capacity among all the tested compositions. This can be related to possible workability loss due to high water absorption capacity of WWF and possible weaker geopolymer-WWF integrated matrix. Interestingly, additional observations indicated that samples incorporating 0.50% and 4.00% wood fiber additives demonstrated comparable flexural strength capacity to the samples with 2.00% fiber content. This suggests that even at lower and higher fiber volume percentages, the flexural strength capabilities remain consistent, further highlighting the potential robustness of the developed materials.

The results were captured in the form of a 7-day flexural strength-displacement plot, which provides a visual representation of the samples' performance characteristics. This plot, recorded and presented in Figure 4.1, offers valuable insights into the mechanical response and structural integrity of the 7-day-old samples prepared with the addition of WWF treated with 2.5M NaOH, thus contributing to a comprehensive understanding of their suitability for specific applications.

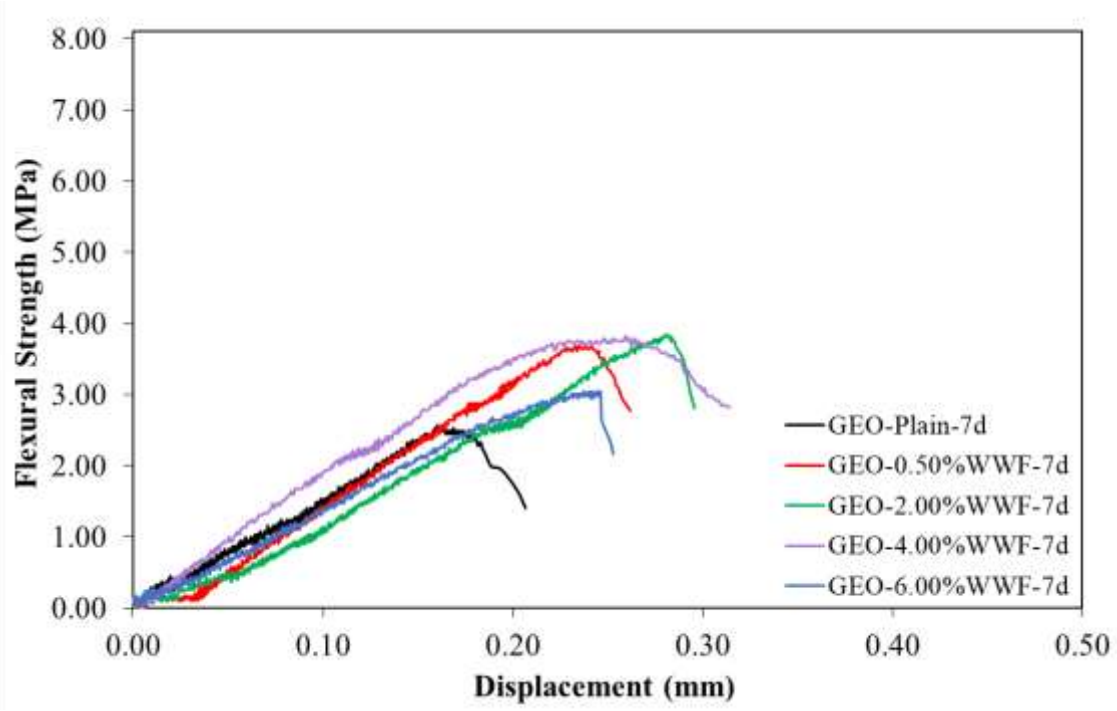

Figure 4.1. Flexural strength-displacement graph of 7-day-old specimens with varying WWF percentages.

The flexural strength-displacement graphs of the 28-day-old samples were meticulously analyzed to evaluate the influence of WWF treated with 2.5M NaOH at various volume percentages, using the GEO specimen with a 2-hour alkali treatment duration. These graphs provide valuable insights into the mechanical performance and structural integrity of the samples over an extended curing period. Compared to the 7-day results and the 28-day flexural strength measurements exhibited a significant increase, indicating the continued development and strengthening of the geopolymer specimens with the passage of time. This enhancement in flexural strength underscores the effectiveness of the WWF treatment and its role in enhancing the overall structural robustness of the samples.

Among the tested samples, it was observed that specimens with WWF-inclusion by 0.50, 2.00, 4.00 and 6.00 vol% displayed 5.56, 5.93, 5.17, 5.31 MPa flexural strength, while displacement values of these specimens were 0.27, 0.41, 0.42, and 0.39 mm, respectively. Notably, the sample containing 2.00% WWF exhibited the highest flexural strength capacity among all the tested compositions, signifying the positive impact of WWF addition on the mechanical performance of the geopolymer specimens. Similar reasons with 7-day results were observed which are related to WWF-matrix integration and high-water absorption capacity of WWF.

To visually depict the flexural strength-displacement characteristics of the 28-day-old samples, a comprehensive flexural strength-displacement plot was generated and is presented in Figure 4.2. This plot provides a clear visualization of the samples' response to applied loads and highlights the improved structural integrity achieved after the prolonged curing period. The detailed analysis of the flexural strength-displacement data and the observed increase in flexural strength over the 28-day period provide valuable insights into the long-term mechanical behavior of the samples incorporating WWF treated with 2.5M NaOH [100].

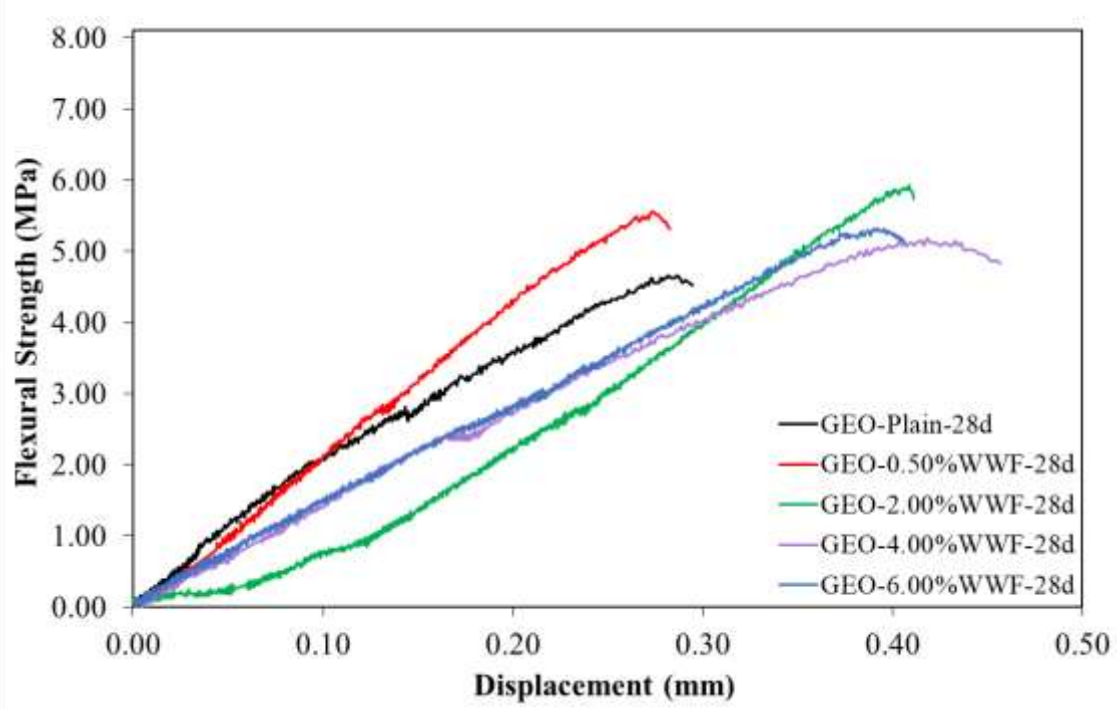

Figure 4.2. Flexural strength-displacement graph of 28-day-old specimens with varying WWF percentages.

4.2 Optimizing PVA Fiber Lengths for Casted Geopolymer

In contrast to WWF, where the feasibility of selecting different lengths was constrained, the evaluation of synthetic fiber involved the testing of three distinct lengths of PVA within the casted samples. To determine the optimal length of PVA and PP fibers among different options, the samples were prepared by incorporating PVA fibers at volume percentages of 0.50% and 1.00% in relation to the precursor. Varying lengths of 6.00, 8.00, and 12.00 mm were selected to assess their influence on the flexural strength and displacement characteristics of the samples. The flexural strength-displacement graphs of the 28-day-old specimens were subjected to meticulous analysis to evaluate the effect of fiber length at different volume percentages. Unveiling the findings from the four-point bending test were presented by calculating the average values obtained from six samples, providing reliable and representative data. The detailed graphical representation of these results can be found in Figure 4.3.

Upon examination of the flexural strength data for samples with a 0.50 vol% inclusion, it was observed that the length of the PVA fibers played a significant role. The 8.00 mm PVA fiber inclusion exhibited a flexural strength of approximately 5.49 MPa, while the 12.00 mm PVA fiber inclusion displayed a flexural strength of approximately 5.13 MPa. In comparison with 6.00 mm PVA fiber length showcased a higher flexural strength of 5.93 MPa. This indicates a decrease of approximately 7.28% and 13.36% for the 8.00 mm and 12.00 mm PVA fiber samples, respectively, when compared to the 6.00 mm PVA fiber sample. Furthermore, a parallel pattern was noted concerning the displacement. The 8.00 mm PVA fiber inclusion resulted in a displacement decrement of 19.69% compared to the 6.00 mm PVA fiber sample, while the 12.00 mm PVA fiber inclusion exhibited a displacement decrement of 37.27% relative to the same reference sample.

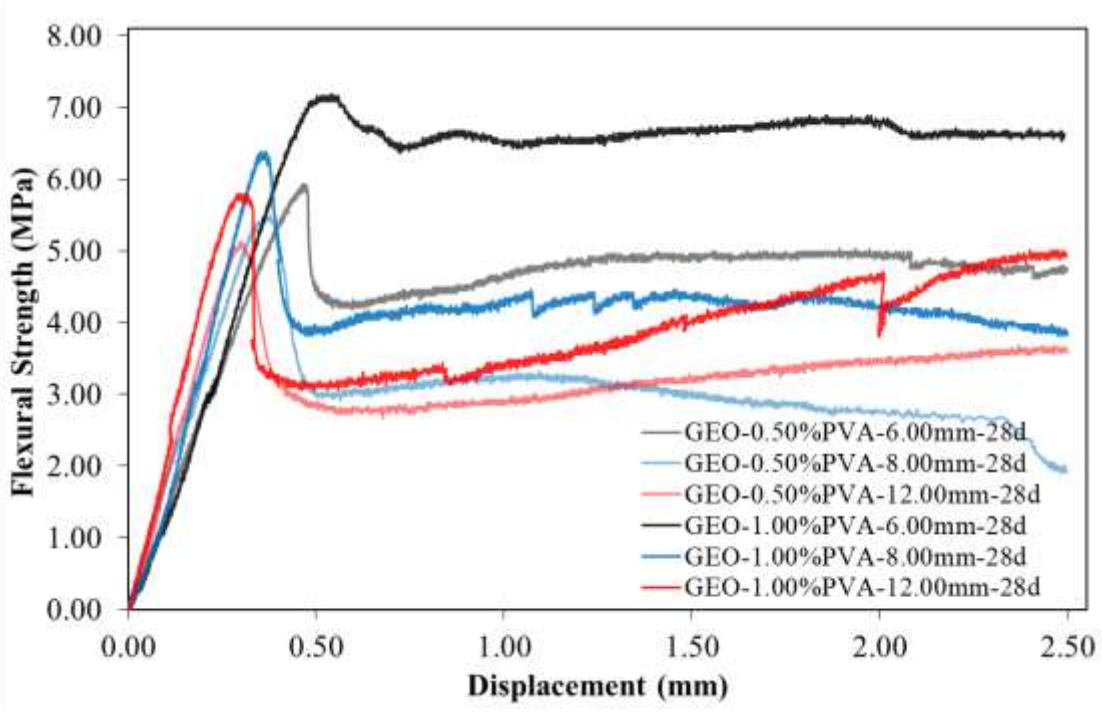

Figure 4.3. Flexural Strength-Displacement Graph for PVA Fiber (6.00, 8.00, 12.00 mm, 0.50% and 1.00% volume) at 28-day.

Even when 1.00% PVA was added, the trend observed for 0.50% PVA inclusion remained unchanged. Geopolymer samples incorporating PVA fibers of different lengths displayed varying flexural strengths at 28-day-old. The 6.00 mm PVA length exhibited approximately

7.19 MPa, while the 8.00 mm and 12.00 mm lengths showed strengths of approximately 6.38 MPa and 5.79 MPa, respectively. This indicates a reduction of around 11.19% and 19.47% in flexural strength for the 8.00 mm and 12.00 mm samples compared to the 6.00 mm ones.

Additionally, a similar pattern emerged in terms of displacement, with reductions of about 34.58% and 45.78% recorded in the 8.00 mm and 12.00 mm PVA-incorporating samples, respectively. These findings underscore the significant impact of PVA volume and length on the flexural strength and displacement characteristics of the geopolymer samples. The observed decrease in flexural strength and displacement suggests that longer lengths of PVA have an adverse effect on the mechanical properties of the geopolymer matrix. These insights play a pivotal role in optimizing the composition and design of geopolymer composites, ensuring their suitability for diverse applications in the construction and engineering domains.
The possible reasons for decrease in flexural strength as the fiber length increases can be: I) heterogenous fiber dispersion, II) fiber orientation, III) possible fiber agglomeration, IV) interfacial bonding and fiber-geopolymer matrix compatibility. Longer PVA fibers may have more difficulty dispersing uniformly within the geopolymer matrix compared to shorter fibers. Inadequate dispersion can lead to clustering or agglomeration of fibers, creating weak points or stress concentrations within the material, which can decrease flexural strength. Followingly, longer PVA fibers could be more likely to form agglomerates or bundles during the mixing process, especially if they are not properly dispersed. These agglomerates can act as stress concentration points, reducing the overall flexural strength of the material. Also, longer fibers such as 12.00 mm PVA may have a greater tendency to align or orient themselves in a specific direction during the mixing and curing process. If the fiber orientation is not optimal for resisting the applied flexural stress, it can result in decreased strength. Moreover, such longer fibers may have a reduced surface area of contact with the geopolymer matrix compared to shorter fibers. This can result in weaker interfacial bonding between the fibers and the matrix, leading to reduced load transfer and lower flexural strength [101][102][103][104][105][106].

4.3 Optimizing PVA Fiber Ratios for Casted Geopolymer

To comprehensively assess the mechanical behavior of samples aged 7 and 28-day, a detailed analysis was undertaken, specifically focusing on the flexural strength-displacement

characteristics. These samples were meticulously prepared using the GEO specimen, incorporating 6.00 mm length PVA fibers at varying volume percentages (0.25, 0.50, 0.75, and 1.00). The flexural strength of the specimens was determined through four-point bending tests, with each value presented in Figure 4.4 representing the average obtained from six sample tests. Graphs depicts the results of the bending loading tests conducted on the specimens, showcasing the effect of PVA fibers on flexural strength. Notably, the flexural strength of the samples demonstrates an overall increase when PVA fibers are incorporated. In the case of the 7-day-old samples, the flexural strength of the PVA fiber-reinforced samples ranged between 29.95% and 59.28% higher than that of the plain sample. However, for the 28-day-old samples, only the samples containing 0.25% PVA fibers exhibited same amount in flexural strength, while in all other cases, the flexural strength of the PVA fiber-reinforced samples exceeded plain samples (Figure 4.5). This observed enhancement in flexural strength can be attributed to the remarkable ability of PVA fibers to bridge cracks and augment the flexural strength capacity of the samples. Consequently, the samples containing PVA fibers displayed significantly improved flexural strength, surpassing that of the plain sample. The most noteworthy increase in flexural strength at 28-day was observed in the sample incorporating 1.00% PVA fibers, exhibiting an impressive increase of approximately 35.26% with 7.19 MPa flexural strength. These findings are consistent with previous research studies, which further substantiate the efficacy of PVA fibers in enhancing the flexural strength of geopolymer composites.

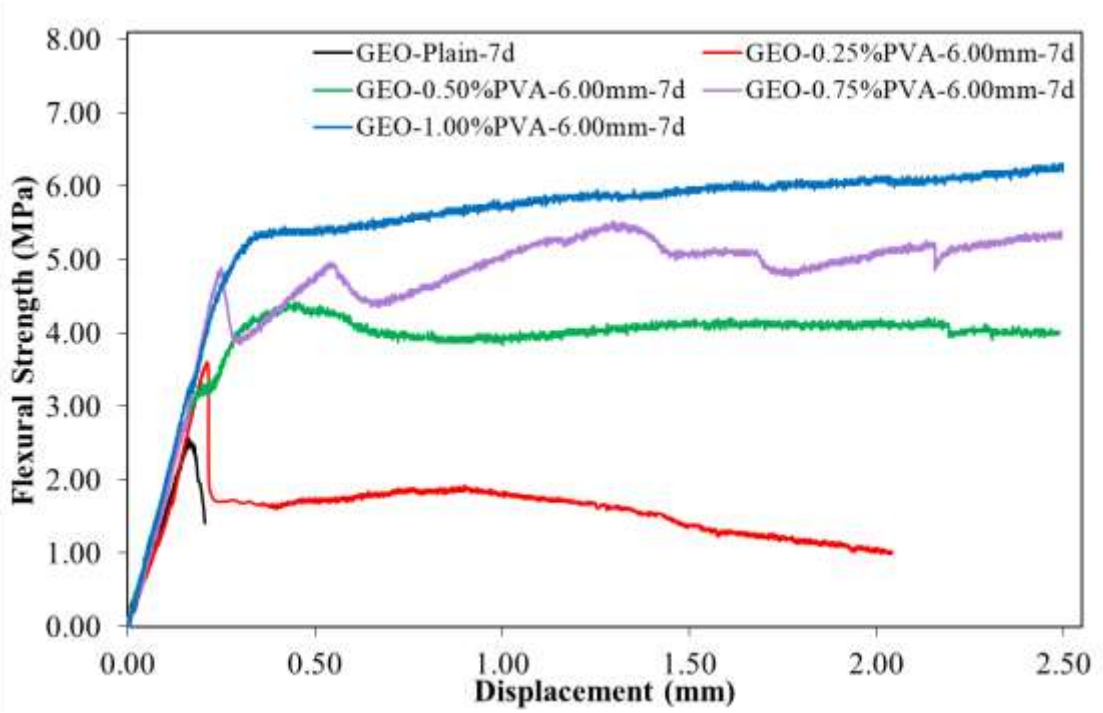

Figure 4.4. Flexural strength-displacement graph of 7-day-old PVA fiber (6.00mm length) with volume percentages of 0.25%, 0.50%, 0.75%, and 1.00%.

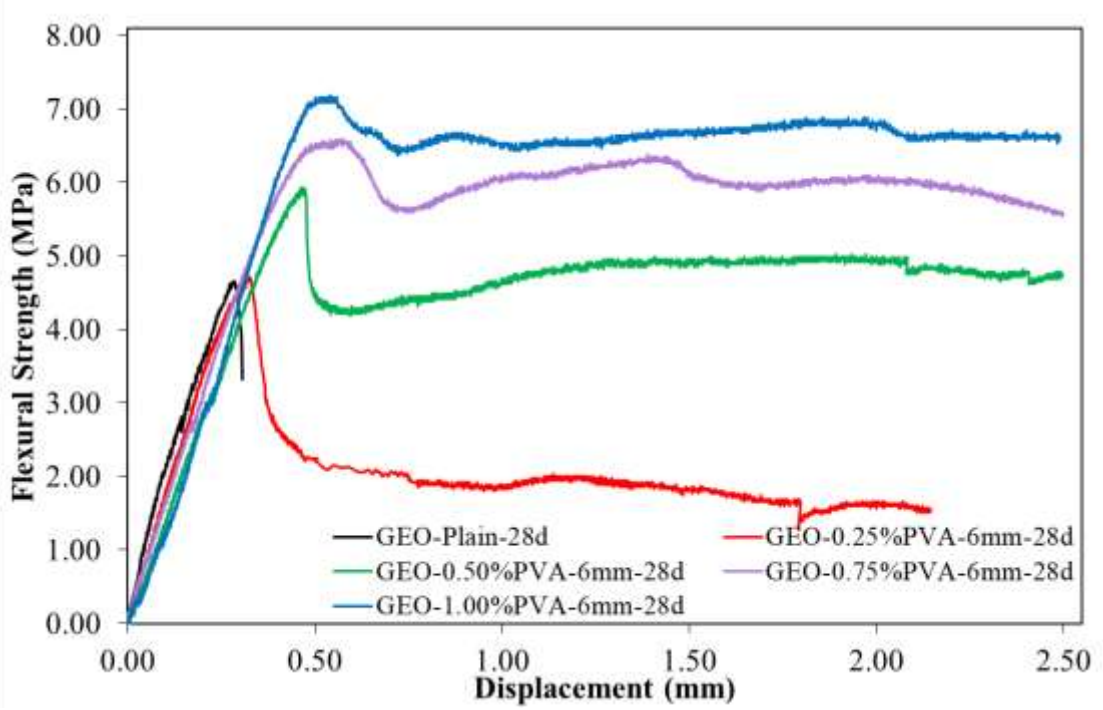

Figure 4.5. Flexural strength-displacement graph of 28-day-old PVA fiber (6.00mm length) with volume percentages of 0.25%, 0.50%, 0.75%, and 1.00%.

Examining Figure 4.4 and Figure 4.5, it is evident that the behavior of the samples with PVA fibers differs from that of the sample without fibers (GEO-Plain). The flexural strength-displacement curves of the PVA fiber-reinforced samples exhibit greater ultimate strength and displacement compared to the sample without fibers. In contrast, the GEO-Plain sample experiences sudden and rapid failure upon reaching its maximum flexural strength capacity, leading to an immediate drop in the flexural strength-displacement diagram. Conversely, the presence of PVA fibers in the samples alters their flexural strength-displacement characteristics, resulting in higher ultimate strength and displacement.

The slope of the force-displacement diagram provides insight into the bending stiffness of the test specimen. By referring to graphs, it becomes apparent that geopolymer composites with PVA fibers possess lower bending stiffness compared to specimens without fibers. Essentially, geopolymer composites with PVA fibers exhibit enhanced mobility in the face of applied force, thus demonstrating greater ductility when compared to ordinary concrete. The possible reasons for these results can be related crack bridging effects of PVA, possible energy absorption and stress transfer properties of PVA, improved fiber-matrix interfacial bonding due to plausible reinforcement behavior of PVA. PVA fibers could bridge across cracks that form within the geopolymer matrix under loading. This bridging effect helps to distribute the applied stress and prevents the cracks from propagating further. As a result, the flexural strength of the composite is increased as fiber amount increases. PVA fibers can also have the ability to absorb and dissipate energy during flexural deformation. The fibers undergo deformation and pull-out from the matrix, absorbing energy in the process. This energy absorption mechanism can contribute to an increase in flexural strength, while enhancing the stress transfer mechanism within the geopolymer matrix. When the material is subjected to flexural loading, the fibers help transfer the applied stress from the matrix to the fibers, reducing the stress concentration and improving the overall strength. Moreover, the addition of PVA fibers can enhance the interfacial bonding by acting as reinforcement within the geopolymer matrix to help distribute the load more evenly and resist crack propagation, between the fibers and the geopolymer matrix. Improved bonding ensures effective load transfer between the fibers and the matrix, resulting in increased flexural strength[102][103][105][106][107][108].

4.4 Optimizing PP Fiber Ratios for Casted Geopolymer

Flexural strength-displacement graphs (Figure 4.6) were plotted for 7-day-old samples prepared with varying volumes (0.25%, 0.50%, 0.75%, and 1.00%) of PP fiber in combination with recipe GEO-mixtures. Among these samples, it was observed that specimens with PP-inclusion by 0.25%, 0.50%, 0.75%, and 1.00% showed 2.85, 3.85, 4.85, 5.03 MPa flexural strength, while displacement values of these specimens were 0.18, 0.26, 0.34, and 0.29 mm, respectively. Notably, the sample containing 1.00% PP fiber exhibited the highest load-bearing capacity. Comparatively, the samples with 0.75% and 0.50% PP fiber additives demonstrated maximum loads they could sustain being approximately 4.85 MPa and 3.85 MPa, respectively. These samples also exhibited displacement values, with approximately 0.34 mm and 0.26 mm, respectively.

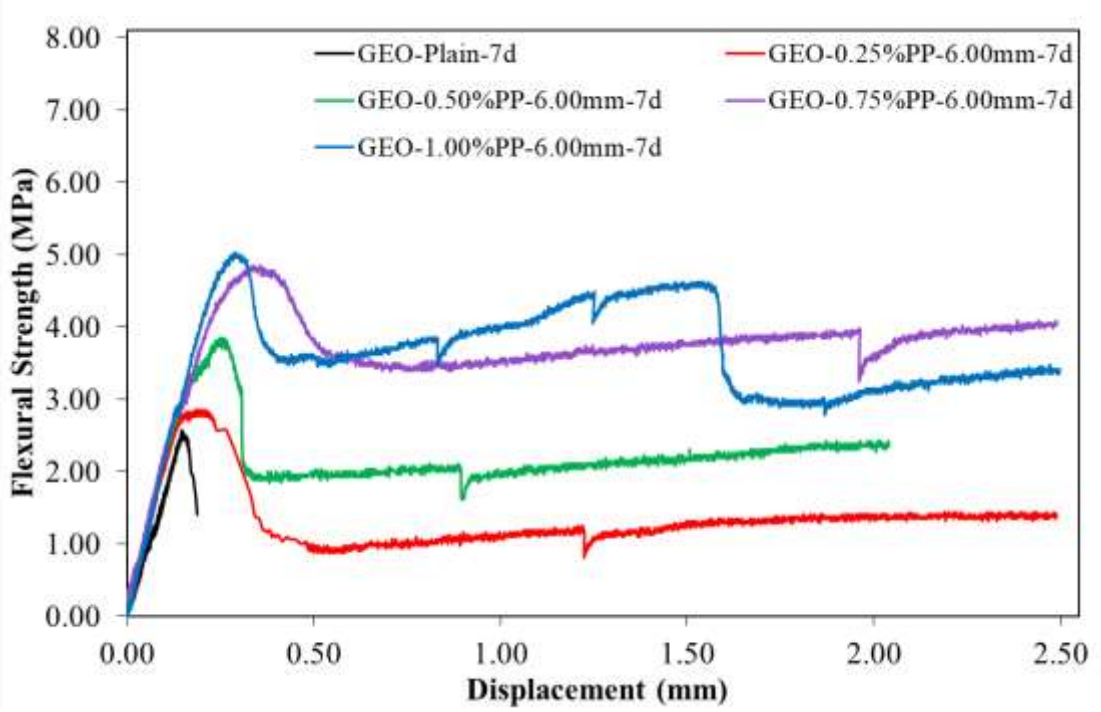

Figure 4.6. Flexural strength-displacement graph of 7-day-old PP fiber (6.00mm length) with volume percentages of 0.25%, 0.50%, 0.75%, and 1.00%.

The flexural strength-displacement graphs of the 28-day-old samples prepared with the addition of PP fiber treated at different volume percentages with GEO mixture were drawn (Figure 4.7); Among these 28-day-old samples, it was observed that specimens with PP-

inclusion by 0.25%, 0.50%, 0.75%, and 1.00% showed 4.89, 5.52, 6.12, 6.42 MPa flexural strength, while displacement values of these specimens were 0.22, 0.28, 0.36, and 0.34 mm, respectively. The 1.00% PP fiber sample showed the highest value. While the samples with the addition of PP fiber in 0.75% ratios show similar trend. Some possible reasons for the overall increase in flexural strength and the reduced increment in the 0.25% sample can be related to fiber reinforcement (by the addition of PP fibers providing reinforcement within the geopolymer matrix, enhancing fibers distribute the load more evenly and helping resist crack propagation), crack bridging (PP fibers can distribute the stress and preventing further crack propagation), fiber-matrix bonding (by forming strong interfacial bonding with the geopolymer matrix, ensuring effective stress transfer between the fibers and the matrix), fiber aspect ratio (the aspect ratio (length to diameter) of the PP fibers can influence their effectiveness in enhancing flexural strength. Higher aspect ratios allow the fibers to span a larger distance within the geopolymer matrix, providing better reinforcement and improved flexural strength. It's possible that the 0.25% sample has a lower aspect ratio, resulting in a lesser increment in flexural strength compared to higher fiber content samples), fiber dispersion and possible saturation effect (where the addition of PP fibers beyond a certain threshold (0.75%) does not contribute significantly to the increase in flexural strength).

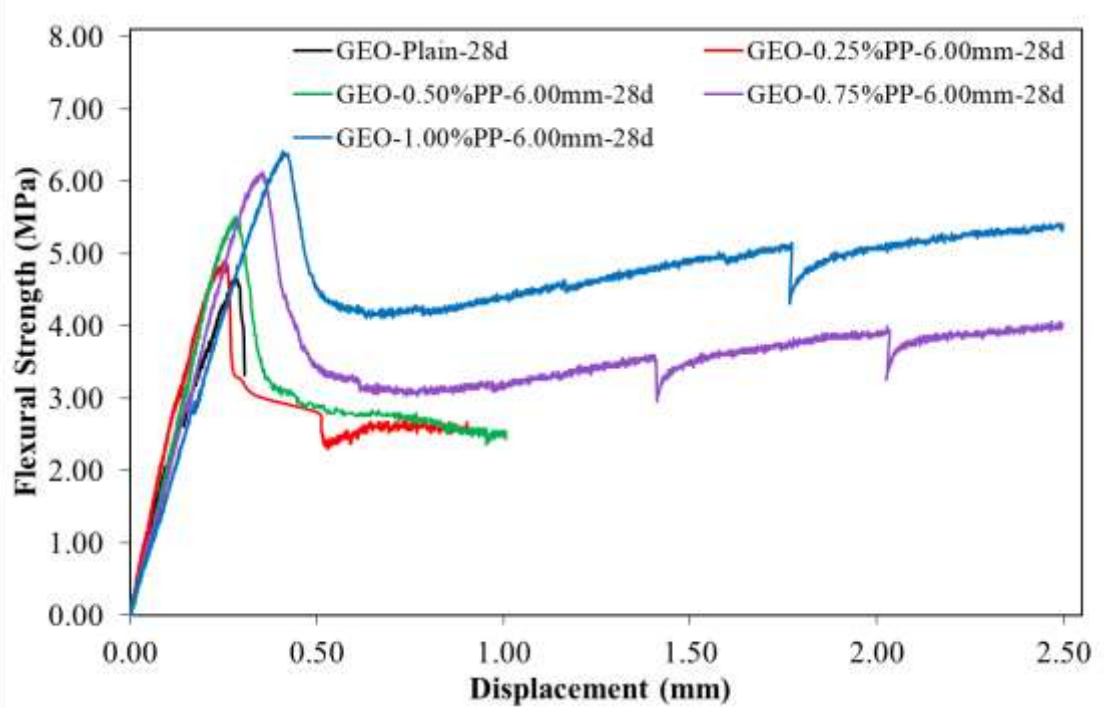

Figure 4.7. Flexural strength-displacement graph of 28-day-old PP fiber (0.25%, 0.50%, 0.75%, 1.00% volume).

4.5 Compressive Strength

Subsequent to the determination of the optimal WWF percentage, the 3D printing process for geopolymer was executed utilizing 2.00% volume. Concurrently, a selection of three proportions, namely 1.00%, 0.75%, and 0.50%, was made for both PVA and PP fibers. It is noteworthy to acknowledge that the endeavor to incorporate 1.00% PVA and PP fibers within the geopolymer matrix was constrained by the formidable challenges posed by high viscosity and limited pumpability. Consequently, the printing process utilizing a pump machine was deemed unfeasible under these conditions. However, the 3D printing procedure was successfully conducted solely with geopolymer compositions containing PVA and PP fibers at the reduced levels of 0.75% and 0.50%.

4.5.1 Effect of WWF on the Compressive Strength

The mechanical characteristics of printed objects, particularly compressive strength, can be affected by the direction of loading. This is due to the 3D-printing process being layer-by-

layer, resulting in an interlayer bond zone between consecutive layers. The mechanical characteristics of this bond interface are often weaker than the core area of the layers, resulting in anisotropy, a performance variance. Anisotropy is caused by the loading and printing directions, resulting in variances in the mechanical performance of the printed objects [110]. Testing for compressive strength was done on specimens created using both mold casting and 3D printing in order to evaluate the anisotropic mechanical properties of the additively manufactured samples and to examine the impact of the process of production on the physical characteristics of geopolymer mortars made completely from CDW. Three alternative loading scenarios, including lateral, parallel, and perpendicular to the printing direction, were used in the experiments. This made it possible to compare the mechanical capabilities of the two manufacturing processes in great detail. The average compressive strength test results of 7-day and 28-day geopolymer casted and printed samples are depicted in Figure 4.8. To investigate the impact of adding WWF on the mechanical properties, two sets of samples were manufactured and prepared for GEO recipe: one without any fiber and another with the addition of 2.00% of WWF. Regardless of loading conditions, the compressive strength test results for the 7-day and 28-day printed specimens consistently exhibited improved mechanical performance when WWF was introduced into the system. Among samples, in terms of the printed specimens, the average of perpendicular-loaded 2.00%WWF samples achieved the highest compressive strength at 28-day, measuring 23.43 MPa. The parallel-loaded samples reached an average compressive strength of 21.04 MPa, while the lateral-loaded sample exhibited a strength of 19.05 MPa. Observing different orders of compressive strength increment ratios in perpendicular, parallel, and lateral loading directions in 3D-printed geopolymer systems incorporating WWF can be influenced by several factors. Fiber alignment and orientation can be one of these factors. In the perpendicular loading direction, the WWFs may be better aligned and oriented to resist the applied compressive forces. The alignment of fibers in this direction allows for efficient load transfer and contributes to increased compressive strength. In the parallel and lateral loading directions, the fibers may have less favorable alignment and orientation, resulting in relatively lower strength increments. Moreover, the load-bearing mechanism can be considered as another factor. WWF could have been acting as load-bearing elements in the geopolymer matrix and help distribute the applied compressive load. In the perpendicular loading direction, where the fibers are

aligned to bear the load, they can effectively resist the forces, leading to higher compressive strength. In the parallel and lateral loading directions, the load-bearing mechanism of the fibers may be less efficient, resulting in lower strength increments. Additionally, fiber-matrix bonding can be evaluated. The bond strength between the WWF and the geopolymer matrix can vary with loading direction. In the perpendicular loading direction, the fibers may have better interfacial bonding with the matrix, enhancing stress transfer and contributing to increased strength. In the parallel and lateral loading directions, the fiber-matrix bonding may be comparatively weaker, leading to lower strength increments. Furthermore, fiber distribution could have been effective. The distribution of WWF within the geopolymer matrix can influence the strength increments in different loading directions. If the fibers are more evenly distributed and well-dispersed in the perpendicular loading direction, their reinforcing effect can be more significant, resulting in higher compressive strength. In the parallel and lateral loading directions, uneven fiber distribution or clustering may limit their contribution to strength improvement [109].

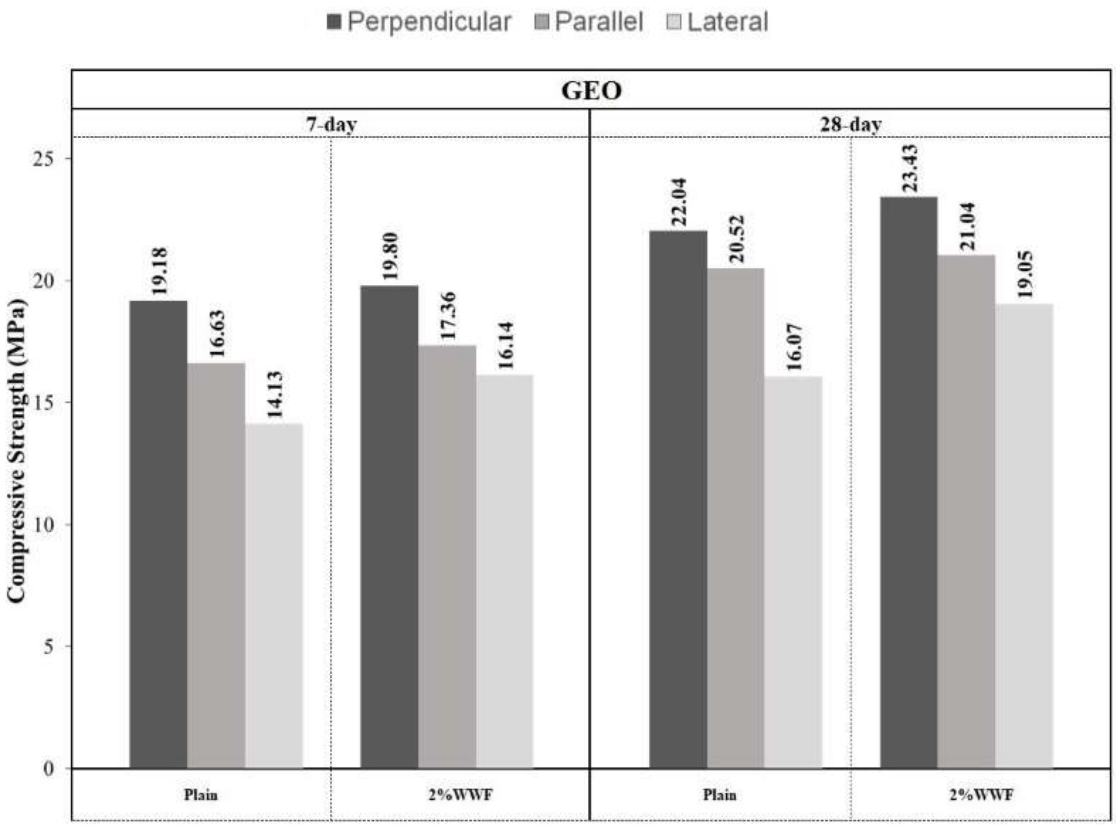

Figure 4.8. Compressive strength of 7-day and 28-day samples (Plain, 2.00% WWF).

4.5.2 Effect of PVA Fiber on the Compressive Strength

In order to further investigate the impact of fiber additives on the geopolymer mixtures, additional experiments were conducted using both PVA fiber and PP fiber in conjunction with GEO mixture. This choice was based on previous studies which demonstrated that these fibers exhibit favorable properties such as enhanced workability and extrudability for the 3D printing process. The objective was to examine the influence of increasing fiber ratios on the compressive strength test results of the mixtures, while keeping other mixture design parameters constant. The findings indicated that increasing the fiber ratio from 0% to 0.50% and from 0.50% to 1.00% led to higher compressive strength values for the specimens. Notably, at lateral direction, the inclusion of 0.50% PVA fibers resulted in a significant increase of approximately 26.79% and 26.41% in compressive strength for the 7-day specimens A similar trend was observed for the 28-day specimens, with a respective increase of approximately 31.03% and 29.21% for the 0.50% and 0.75% PVA fiber ratios (Figure 4.9). These findings highlight the positive effect of incorporating PVA fibers on the mechanical performance of the geopolymer mixtures. The increased compressive strength observed with higher fiber ratios suggests improved structural integrity and resistance to applied load.

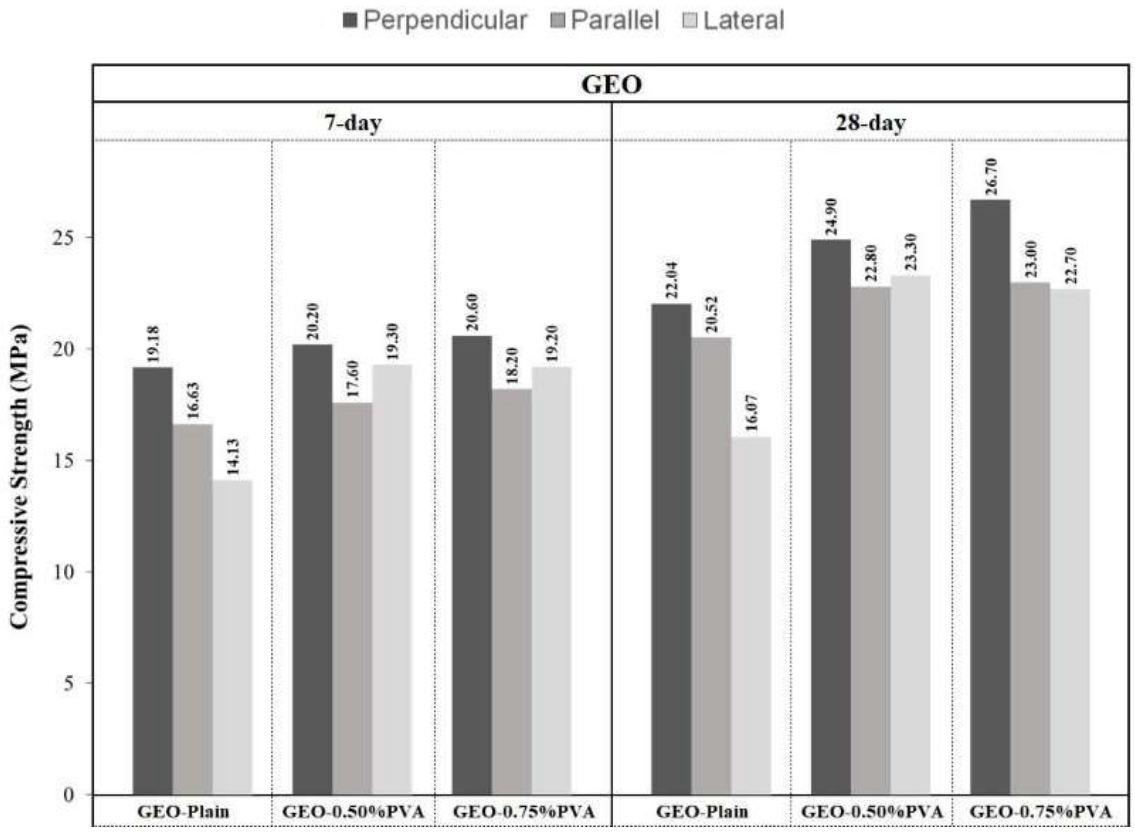

Figure 4.9. 7-day and 28-day compressive strength of samples (Plain, 0.50% and 0.75% PVA).

4.5.3 Effect of PP Fiber on the Compressive Strength

The compressive strength test results printed specimens, as depicted in Figure 4.10, exhibited consistent trends when utilizing PVA fiber mixtures. The findings demonstrated that incorporating fiber ratios of 0.50% and 0.75% led to superior compressive strength values compared to specimens without fibers. Notably, in the lateral direction, the inclusion of 0.50% PP fibers resulted in a significant increase of approximately 18.23% and 21.63% in compressive strength for the 0.50% and 0.75% specimens, respectively, within the 7-day period. Similar observations were made for the 28-day specimens, with respective increases of approximately 28.19% and 29.61% for the 0.50% and 0.75% PP fiber ratios. These improvements can be attributed to the crack-bridging effect and prevention of material splitting facilitated by the fibers. In the lateral direction, where the printed layers are stacked, the fibers play a crucial role in maintaining interlayer cohesion. This becomes particularly significant in cases where layer alignment is imperfect, as the fibers fill in gaps and contribute

to enhanced strength. Furthermore, the fibers aid in distributing stress more uniformly throughout the material, thereby mitigating the risk of localized failure. By serving as load-bearing elements, the fibers effectively alleviate the load imposed on the surrounding material, resulting in improved mechanical performance.

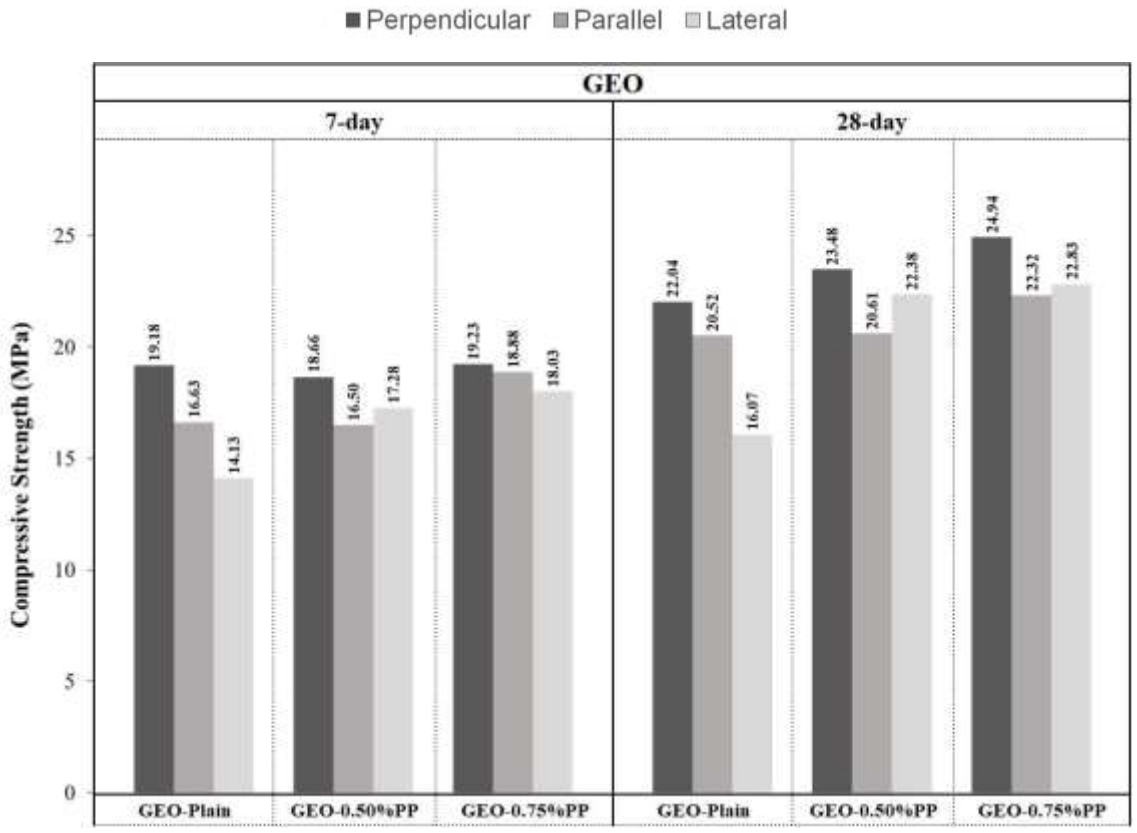

Figure 4.10. 7-day and 28-day compressive strength of geopolymer samples (Plain, 0.50% and 0.75% PP).

4.6 Flexural Strength

The flexural strength of 3D-printed specimens of CDW-based geopolymer mortar was investigated to compare the performance of layered samples with different fibers. The specimens were loaded in directions that were both lateral to and perpendicular to the printing route. The objective was to investigate the impact of fibers concentration on the flexural

performance of the mixes. The average flexural strength test outcomes 3D-printed specimens that were cured in ambient conditions for 7 and 28-day are shown in Figure 4.11. Due to the continuing geopolymerization process, the mixes' flexural performance continuously improved with increasing curing age. After 28-day ambient curing, the geopolymer mortar mixtures with a PVA fiber content ratio of 0.75% exhibited the highest maximum flexural strength results for perpendicular-loaded, and lateral-loaded 3D-printed specimens. The average flexural strength for the lateral-loaded 3D-printed specimens reached a maximum value of 8.76 MPa, while the perpendicular-loaded 3D-printed specimens had maximum values of 8.02 MPa. The flexural strength results of the 3D-printed specimens with WWF, both in the perpendicular and lateral loading directions, were in agreement with several research findings [85][99] [111][112][113][114][115][116][117].

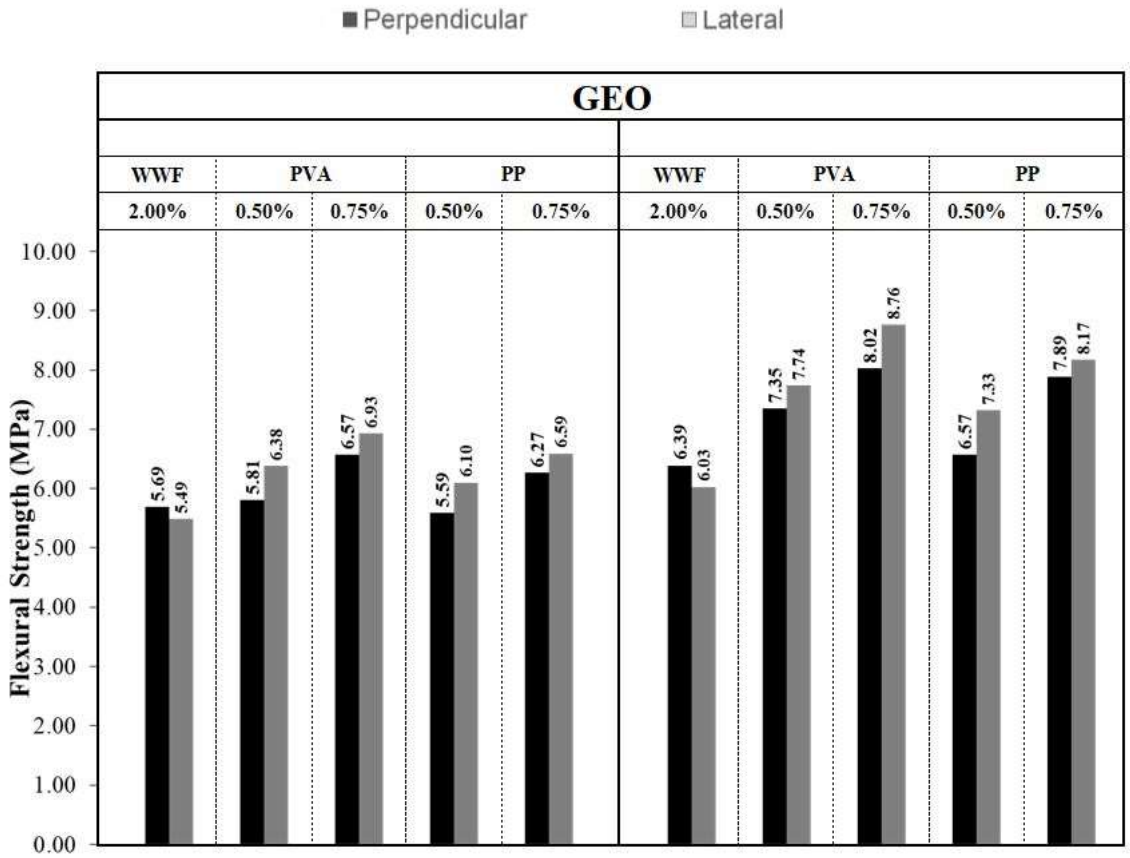

Figure 4.11. Flexural strength of 3D-printed samples (WWF, PVA, PP fiber combinations).

The results clearly demonstrated that the flexural strength of the 3D-printed specimen with WWF loaded perpendicular to the nozzle direction of movement was higher than that of the lateral-laden 3D-printed specimens. Contrarily result obviously illustrate that the flexural strength of the 3D-printed specimen containing PVA and PP fibers loaded at lateral to the direction of movement was higher than two named specimens. In contrast, the results clearly indicate that the 3D-printed specimen containing PVA and PP fibers, loaded laterally to the direction of movement, exhibited higher flexural strength than WWF specimens.

4.6.1 Effect of Various Fibers on Flexural Strength

In comparison to specimens containing 0.50% PVA fibers, the specimens containing 0.75% PVA fibers shown an increase in flexural strength in the lateral direction of roughly 7.94% and 11.64% at 7-day and 28-day, respectively. Following that, the specimens with 0.75% PP fibers compere to the 0.50% PP fibers exhibited a growth rate of approximately 7.44% and 10.28% for 7-day and 28-day, respectively.

The bending strength of the samples was significantly affected by the fiber addition and increased noticeably when compared to the plain samples. While the use of a two percent volume ratio of WWF resulted in notable improvements, the results were nearly equivalent to those obtained with PVA and PP fibers at a 0.50% volume percentage. This can be attributed to the inherent properties of synthetic fibers, such as PVA and PP, which offer superior performance in terms of flexural strength. Synthetic fibers generally outperform natural fibers like WWF in construction materials due to several advantages. Firstly, synthetic fibers exhibit higher tensile strength, enabling them to withstand greater loads before failure. This characteristic greatly contributes to the enhanced flexural strength observed in the samples. Secondly, synthetic fibers possess superior durability, as they are more resistant to degradation caused by moisture, chemicals, and biological agents. They maintain their structural integrity over a longer period, resulting in improved long-term performance. Consistent quality is another advantage of synthetic fibers. They can be manufactured to possess uniform quality and properties, ensuring consistent reinforcement throughout the material. On the other hand, natural fibers may exhibit inherent variability due to differences in their source, growth conditions, and processing.

Furthermore, synthetic fibers exhibit excellent compatibility with various matrix materials, including concrete or polymers, facilitating efficient load transfer and effective reinforcement. This compatibility contributes to the overall enhancement of flexural strength. It is important to note that the selection of fiber type depends on the specific application and requirements. Natural fibers like WWF may offer certain advantages in terms of eco-friendliness or thermal properties. However, when considering flexural strength, synthetic fibers such as PVA and PP tend to yield superior results.

4.6.2 Mechanical Properties Dependent on Direction

In addition to looking at the impacts of the fibers, the mixes' flexural performance was also evaluated as part of the investigation of their anisotropic behavior. The test outcomes showed that at each testing age, the flexural strength of the 3D-printed specimens was either comparable to or greater than that of the mold-casted specimens. It was previously anticipated that the flexural strength of the 3D-printed samples would decrease as a result of the layer-by-layer fabrication process. Contrary to predictions, however, the flexural strength increased, which may be attributed to the mixes' greater compaction, made possible by the high-pressured pump. It is vital to notice that the specimens' air void content significantly influences their flexural strength [120]. As produced CDW-based geopolymer has a sticky character due to clay origins, more air void formation was found in the geopolymer specimens during casting compared to the 3D-printed geopolymer specimens [118][119]. Due to the weight of the top layer and the pushing force exerted by the pressured subsequent materials from the pump, the compacting of the bottom layer of prismatic specimens was enhanced during printing. It is crucial to recognize that elements connected to the production process have a significant impact on how well the mixes work. Manufacturing-related issues have a significant impact on how CDW-based geopolymer mortar mixes function. Furthermore, the performance of the 3D-printed specimen is significantly influenced by the way in which loads are distributed across it. The 3D-printed specimens loaded perpendicularly displayed more flexural strength than the one loaded laterally, according to the data, for each combination and testing age. This is because the initial layer, which was more compacted and bonded, was situated in the tension zone, which led to better performance, during flexural strength testing

in the perpendicular direction. Figure 4.5a shows a fracture behavior that closely resembles the perpendicular reference line when the fracture behaviors are examined. Figure 4.5b, on the other hand, shows fracture behavior that initially follows the reference line until it reaches the bond region, at which point it diverges. Considering the printing direction, a weakness in this area can cause a divergence in the crack path and a loss of up to 29% of flexural strength.

4.7 Direct Tensile Strength

The outcome of the direct tensile tests performed on a number of printed samples stored at ambient conditions for 7 and 28 days are depicted in Figure 4.12. Analyzing the figure reveals that the bond strength of the combinations exhibited a continuous increase as the curing ages extended, primarily due to the ongoing geopolymerization reaction. Notably, the specimens containing 0.75% PVA fiber demonstrated the highest strength among all the samples tested in geopolymer mortars, particularly regarding the direct tensile strength of the 28-day samples. Following a 28-day period of curing, the direct tensile strength outcomes peaked at an impressive value of 2.41 MPa. Interestingly, when examining the 7-day results, there were no discernible differences observed between PVA and PP fibers with ratios of 0.50% and 0.75%. Figure 4.13 reveals that there was not any noticeable difference in the tensile strength of 3D-printed geopolymer specimens that contain 0.50% and 0.75% fiber at 7-day. Meanwhile, at 28-day, the tensile strength of the specimens containing 0.75% fiber was significantly higher than the specimens containing 0.50% fiber. The tensile strength of the 0.75% fiber specimens was 20.44% higher for PVA fibers and 8.43% higher for PP fibers. These result show that the addition of fibers to 3D printing materials can significantly improve the bond strength and tensile strength of the printed parts. This is because the fibers help to distribute the load more evenly throughout the part, and they also help to prevent cracks from forming. As a result, parts that contain fibers are less likely to break or deform under load.

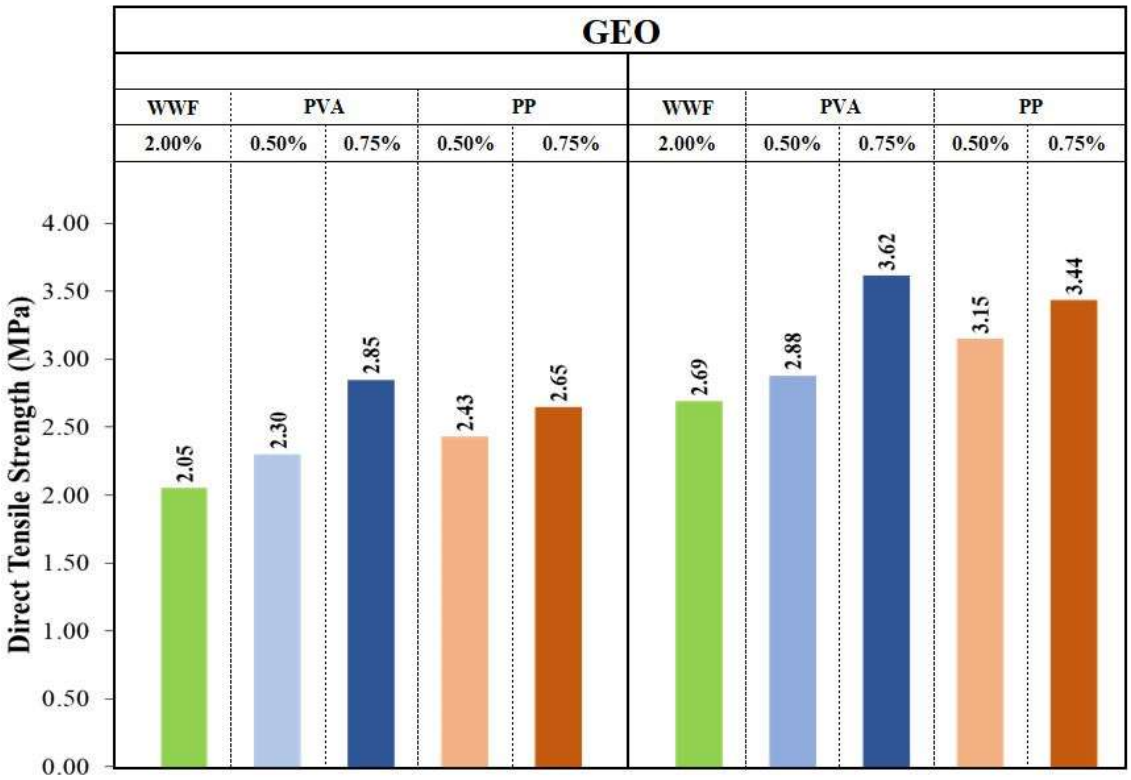

Figure 4.12. Direct tensile strength of 3D-printed samples (WWF, PVA, PP combinations).

The addition of fibers to 3D printing materials has been found to enhance bond strength and tensile strength due to several specific reasons. Firstly, fibers help bridge the gaps between layers. During the layer-by-layer deposition process of 3D printing, small gaps can form between the layers, weakening the bond and making the part prone to cracking. The inclusion of fibers effectively bridges these gaps, resulting in improved bond strength between the layers. Secondly, fibers aid in distributing the load evenly. Without fibers, the load applied to a 3D printed part may not be uniformly distributed, leading to potential cracks. However, the incorporation of fibers helps evenly distribute the load, mitigating crack formation. Lastly, fibers act as barriers against crack propagation. Should a crack develop in a 3D printed part, fibers impede its growth by acting as a barrier and slowing down its propagation.

Moreover, factors such as the shape and orientation of the fibers also impact tensile strength. Specifically, fibers aligned in the direction of the load provide superior reinforcement compared to randomly oriented fibers. Overall, the addition of fibers to 3D printing materials

significantly enhances both bond strength and tensile strength, imparting resistance against deformation and breakage under load, thereby improving durability.

On the other hand, increasing the quantity of fibers in a 3D printing material expands the available surface area for bonding between the fibers and the matrix. Consequently, this can enhance the bond strength between the fibers and the matrix, leading to a stronger part. However, there is a threshold beyond which adding more fibers may diminish bond strength. This is because the increased fiber content also elevates stress on the bond between fibers and the matrix, eventually causing bond failure and weakening the part. Furthermore, excessive fiber addition can impede the even distribution of fibers within the material, creating weak spots that further reduce bond strength. For WWF specifically, an increase in fiber content has been observed to decrease compressive strength. This decrease is attributed to the inhomogeneous distribution of wood fibers within the system and the high-water absorption capacity of the fibers.

In conclusion, the incorporation of fibers in 3D printing materials provides multiple benefits, including improved bond strength, enhanced tensile strength, increased resistance to deformation and breakage, and overall durability. However, care should be taken not to exceed the optimal fiber quantity, as excessive fiber content may lead to reduced bond strength and uneven fiber distribution, compromising the integrity of the printed part.

5. CONCLUSIONS

This thesis study focused on evaluating the performance of 3D-printed CDW-based geopolymer with different natural and synthetic fibers, considering direction-dependent effects. Additionally, the study aimed to determine the optimal fiber ratio and length for enhancing the mechanical characteristics, including compressive, flexural, direct tensile strength, of 3D-printed geopolymer mortars. A comparison was made between the performances of 3D-printed and mold-casted specimens to assess variations in mechanical properties due to the manufacturing method. Various fiber types, including WWF with ratios of 0.50, 2.00, 4.00, and 6.00% by volume, and PVA and PP fibers with ratios of 0.25, 0.50, 0.75, and 1.00% in three different lengths (6.00mm, 8.00mm, and 12.00mm), were examined in both 3D-printed and mold-casted specimens. The manufactured samples were subjected to mechanical tests, including compressive and flexural strength tests in different loading directions, to determine their anisotropic behavior.

Several findings were drawn from the experiments undertaken to investigate:

- The analysis of 7-day-old samples in terms of flexural strength-displacement characteristics revealed important findings. The incorporation of WWF treated with 2.5M NaOH at different volume percentages resulted in varying load capacities and displacements. Among the tested compositions, the sample containing 2.00% wood fiber exhibited the highest load capacity. Notably, samples with 0.50% and 4.00% wood fiber additives showed comparable load capacities to the 2.00% fiber content, indicating consistent load-bearing capabilities across different fiber volume percentages.

- The analysis of the flexural strength-displacement graphs of the 28-day-old samples incorporating WWF treated with 2.5M NaOH revealed a noticeable increase in flexural strength compared to the 7-day measurements. The samples exhibited an average maximum flexural strength of approximately 5.93 MPa and displayed improved structural integrity. The sample containing 2.00% WWF demonstrated the highest load capacity, indicating the positive impact of fiber addition. The generated flexural

strength-displacement plot visually represented the samples' response to applied loads, highlighting the enhanced mechanical performance achieved over the prolonged curing period. The results of this study contribute significantly to enhancing the comprehensive understanding of the enduring mechanical characteristics and the advantageous outcomes obtained through the treatment of WWF in geopolymer materials.

- The analysis of the flexural strength-displacement graphs of the 28-day-old specimens incorporating PVA fibers at different volume percentages and lengths provided valuable insights into the optimal fiber length. For samples with a 0.50% volume inclusion, the length of PVA fibers played a significant role. The 6.00 mm fiber length demonstrated the highest flexural strength of 5.93 MPa, while the 8.00 mm and 12.00 mm lengths exhibited lower flexural strengths of approximately 5.49 MPa and 5.13 MPa, respectively. This indicates a decrease in flexural strength as the fiber length increases. Similar trends were observed in displacement, with longer fiber lengths resulting in decreased displacements compared to the 6.00 mm reference sample. These findings highlight the importance of selecting the appropriate fiber length to optimize the flexural strength and displacement characteristics of geopolymer specimens incorporating PVA fibers.

- The analysis of the geopolymer samples incorporating PVA fibers at different lengths demonstrated that longer fiber lengths (8.00 and 12.00mm) resulted in reductions in flexural strength and displacement compared to the 6.00 mm length. This indicates the significant influence of PVA fiber volume and length on the mechanical properties of the geopolymer matrix. The findings highlight the importance of selecting appropriate PVA fiber lengths to optimize the flexural strength and displacement characteristics of geopolymer composites in construction and engineering applications.

- The incorporation of PVA fibers in geopolymer composites has shown significant improvements in flexural strength and displacement characteristics. The analysis of samples aged 7 and 28-day revealed that the flexural strength of PVA fiber-reinforced samples was higher compared to samples without fibers. The PVA fibers acted as

crack bridging agents, enhancing the load-bearing capacity and resulting in increased flexural strength. The maximum increment in flexural strength at 28-day was observed in samples containing 1.00% PVA fibers. The flexural strength-displacement curves of PVA fiber-reinforced samples exhibited greater ultimate strength and displacement, indicating improved structural performance and ductility compared to samples without fibers. These findings validate the impact of PVA fibers in enhancing the mechanical properties of geopolymer composites and support their potential application in construction and engineering.

- The evaluation of flexural strength-displacement characteristics of 7-day-old and 28-day-old samples incorporating PP fibers revealed significant improvements in flexural strength- displacement values. At 7-day samples with 1.00% PP fiber demonstrated the highest load capacity. For 28-day-old samples, the average maximum load capacity increased, with the 1.00% PP fiber sample again showing the highest value. Similarly, the 0.75% PP fiber samples displayed a consistent trend. These findings highlight the positive impact of PP fibers on enhancing the flexural strength and displacement characteristics of the samples, indicating their potential use in structural applications.

- In conclusion, the compressive strength test results of both mold-casted and printed specimens consistently showed that incorporating PVA fiber mixtures led to superior strength compared to specimens without fibers. Particularly, the inclusion of 0.50% PP fibers resulted in significant increases in compressive strength within the 7-day and 28-day periods. These improvements can be attributed to the crack-bridging effect and prevention of material splitting facilitated by the fibers. In the lateral direction, where the printed layers are stacked, the fibers play a crucial role in maintaining interlayer cohesion and enhancing strength, especially in cases of imperfect layer alignment. Additionally, the fibers contribute to distributing stress more uniformly, reducing the risk of localized failure. By acting as load-bearing elements, the fibers effectively alleviate the load on the surrounding material, resulting in improved mechanical performance.

- In summary, the addition of synthetic fibers, particularly 0.75% PVA and 0.75% PP fibers, significantly improved the flexural strength of the specimens in the lateral direction. Synthetic fibers, such as PVA and PP, offer superior performance in terms of flexural strength compared to natural fibers like WWF. Synthetic fibers have higher tensile strength, better durability, consistent quality, and excellent compatibility with matrix materials. While natural fibers may have their advantages, synthetic fibers are more effective in enhancing flexural strength. The choice of fiber type should consider specific application requirements.

- the addition of fibers, particularly 0.75% PVA fibers, significantly improves the bond strength and tensile strength of 3D-printed specimens in geopolymer mortars. The ongoing geopolymerization reaction contributes to the continuous increase in bond strength with curing age. The specimens with 0.75% PVA fiber demonstrate the highest strength, especially in the direct tensile strength of the 28-day samples. The inclusion of fibers helps distribute the load evenly, bridge gaps between layers, and act as barriers against crack propagation. Factors such as fiber shape and orientation also impact tensile strength, with aligned fibers providing superior reinforcement. However, there is a threshold beyond which adding more fibers may diminish bond strength, and excessive fiber content can impede even fiber distribution. Careful consideration of fiber quantity is necessary to maintain optimal strength and durability.

6. REFERENCES

[1] A.P. Gursel, C. Ostertag, Comparative life-cycle impact assessment of concrete manufacturing in Singapore, The International Journal of Life Cycle Assessment, 22 (**2017**) 237-255.

[2] Monteiro, P. J., Miller, S. A. and Horvath, A., Towards sustainable concrete. Nature materials, 16(7) (**2017**) 698-699.

[3] S.A. Miller, F.C. Moore, Climate and health damages from global concrete production, Nature Climate Change, 10 (**2020**) 439-443.

[4] Batool, S. A., Iqbal, J., & Ahmad, I. (2021). Environmental and Economic Considerations in Cement Manufacturing. Environment, Development and Sustainability, 1–26.

[5] Tiwary, A., & Mishra, P. K. (**2012**). Environmental and Health Impacts of Cement Manufacturing. Current Science, 102(9), 1211–1217.

[6] U.G. Survey, Mineral commodity summaries, US Geological Survey, 198 (**2019**) 2011.

[7] M. Taylor, C. Tam, D. Gielen, Energy Efficiency and CO2 Emissions from the Global Cement Industry, 50 (**2006**).

[8] Chinda, T. Construction and Demolition Waste Generation and Management Practices during Building Construction: A Case Study. Journal of Environmental and Public Health, (**2016**), 3287912.

[9] M.M. Sabai, M.G.D.M. Cox, R.R. Mato, E.L.C. Egmond, J.J.N. Lichtenberg, Concrete block production from construction and demolition waste in Tanzania, Resources, Conservation and Recycling, 72 (**2013**) 9-19.

[10] Poon, C. S., Yu, A. T. W., & Ng, L. H. W. Comparison of Environmental Implications of Concrete Debris and Reinforced Concrete Debris: A case study in Hong Kong. Construction and Building Materials, 15(6-7), (**2001**). 351-357.

[11] Wu, H., Zuo, J., Yuan, H., Zillante, G. and Wang, J., A review of performance assessment methods for construction and demolition waste management. Resources, Conservation and Recycling, 150 (**2019**) 104407.

[12] B. García de Soto, I. Agustí-Juan, J. Hunhevicz, S. Joss, K. Graser, G. Habert, B. Adey, Productivity of digital fabrication in construction: Cost and time analysis of a robotically built wall, Automation in Construction, 92 (**2018**).

[13] E. Lloret, A.R. Shahab, M. Linus, R.J. Flatt, F. Gramazio, M. Kohler, S. Langenberg, Complex concrete structures: Merging existing casting techniques with digital fabrication, Computer-Aided Design, 60 (**2015**) 40-49.

[14] P. Shakor, J. Sanjayan, A. Nazari, S. Nejadi, Modified 3D printed powder to cement-based material and mechanical properties of cement scaffold used in 3D printing, Construction and Building Materials, 138 (**2017**) 398-409.

[15] Maas, G. and van Gassel, F., The influence of automation and robotics on the performance construction. Automation in construction, 14(4) (**2005**) 435-441.

[16] Nematollahi, B., Xia, M. and Sanjayan, J., Current progress of 3D concrete printing technologies. In ISARC. Proceedings of the International Symposium on Automation and Robotics in Construction. IAARC Publications, 34 (**2017**) 1-8.

[17] Tay, Y.W.D., Panda, B., Paul, S.C., Mohamed, N.A.N., Tan, M.J. and Leong, K.F., 3D printing trends in building and construction industry: A review. Virtual and Physical Prototyping, 12 (**2017**) 261-276

[18] Meyer, C., The greening of the concrete industry. Cement and concrete composites, 31(8) (**2009**) 601-605.

[19] Aïtcin, P., Cements of yesterday and today. Cement and Concrete Research, 30(9) (**2000**) 1349-1359.

[20] Gursel, A.P., Masanet, E., Horvath, A. and Stadel, A., Life-cycle inventory analysis of concrete production: a critical review. Cement and Concrete Composites, 51 (**2014**) 38-48.

[21] Imbabi, M.S., Carrigan, C. and McKenna, S., Trends and developments in green cement and concrete technology. International Journal of Sustainable Built Environment, 1 (**2012**) 194-216.

[22] Sabir, B. B., Wild, S. and Bai, J., Metakaolin and calcined clays as pozzolans for concrete: a review. Cement and concrete composites, 23(6) (**2001**) 441-454.

[23] Cachim, P., Velosa, A. L. and Ferraz, E., Substitution materials for sustainable concrete production in Portugal. KSCE Journal of Civil Engineering, 18(1) (**2014**) 60-66.

[24] McKelvey, D., Sivakumar, V., Bell, A. and McLaverty, G., Shear strength of recycled construction materials intended for use in vibro ground improvement. Proceedings of the Institution of Civil Engineers-Ground Improvement, 6(2) (**2002**) 59-68.

[25] Al Bakri, M. M., Mohammed, H., Kamarudin, H., Niza, I. K. and Zarina, Y., Review on fly ash-based geopolymer concrete without Portland Cement. Journal of engineering and technology research, 3(1) (**2011**) 1-4

[26] Davidovits, J "Geopolymer Chemistry and Applications" Ed. Geopolymer Institute, Saint Quentin, France, (**2008**)

[27] Davidovits, J.,''Geopolymers and Geopolymeric Materials,'' (**1989**) J. Therm. Anal., 35:429–41

[28] Sambucci, M.; Sibai, A.; Valente, M. Recent advances in geopolymer technology. A potential eco-friendly solution in the construction materials industry: A review. J. Compos. Sci. (**2021**), 5, 109.

[29] Duxson, P.; Lukey, G.C.; Separovic, F.; van Deventer, J.S.J. Effect of alkali cations on aluminum incorporation in geopolymeric gels. Ind. Eng. Chem. Res. (**2005**), 44, 832–839.

[30] Liew, Y.M.; Heah, C.Y.; Kamarudin, H. Structure and properties of clay-based geopolymer cements: A review. Prog. Mater. Sci. (**2016**), 83, 595–629.

[31] Hajimohammadi, A., Provis, J. L. and Van Deventer, J. S., Effect of alumina release rate on the mechanism of geopolymer gel formation. Chemistry of Materials, 22(18) (**2010**) 5199-5208.

[32] Hajimohammadi, A., Provis, J. L. and van Deventer, J. S., The effect of silica availability on the mechanism of geopolymerisation. Cement and Concrete Research, 41(3) (**2011**) 210-216.

[33] White, C. E., Provis, J. L., Bloomer, B., Henson, N. J. and Page, K., In situ X-ray pair distribution function analysis of geopolymer gel nanostructure formation kinetics. Physical Chemistry Chemical Physics, 15(22) (**2013**) 8573-8582.

[34] White, C. E., Provis, J. L., Proffen, T. and van Deventer, J. S., Molecular mechanisms responsible for the structural changes occurring during geopolymerization: multiscale simulation. American Institute of Chemical Engineers journal, 58(7) (**2012**) 2241-2253.

[35] Fernández-Jiménez, A., Palomo, A., Sobrados, I. and Sanz, J., The role played by the reactive alumina content in the alkaline activation of fly ashes, Microporous and Mesoporous Materials, 91 (**2006**) 111-119.

[36] Nergis, D.D.B.; Abdullah, M.M.A.B.; Vizureanu, P.; Tahir, M.F.M. Geopolymers and Their Uses: Review. IOP Conf. Series: Mater. Sci. Eng. (**2018**), 374, 012019.

[37] Duxson, P., Fernández-Jiménez, A., Provis, J. L., Lukey, G. C., Palomo, A. and van Deventer, J. S., Geopolymer technology: the current state of the art. Journal of materials science, 42(9) (**2007**) 2917-2933.

[38] Provis, J. L. and Bernal, S. A., Geopolymers and related alkali-activated materials. Annual Review of Materials Research, 44 (**2014**) 299-327.

[39] Provis, J. L. and Bernal, S. A., Milestones in the analysis of alkali-activated binders. Journal of Sustainable Cement-Based Materials, 4(2) (**2015**) 74-84.

[40] Shi, C., Qu, B. and Provis, J. L., Recent progress in low-carbon binders. Cement and Concrete Research, 122 (**2019**) 227-250.

[41] Poon, C. S., Ann, T. W. and Ng, L. H., On-site sorting of construction and demolition waste in Hong Kong. Resources, conservation and recycling, 32(2) (**2001**) 157-172.

[42] Ahmari, S., Ren, X., Toufigh, V. and Zhang, L., Production of geopolymeric binder from blended waste concrete powder and fly ash. Construction and Building Materials, 35 (**2012**) 718-729.

[43] B. Nematollahi, M. Xia, S.H. Bong, J. Sanjayan, Hardened properties of 3D printable ‘one-part’geopolymer for construction applications, RILEM International Conference on Concrete and Digital Fabrication, Springer, (**2018**), pp. 190-199.

[44] Khater, H. M., Effect of calcium on geopolymerization of aluminosilicate wastes. Journal of materials in civil engineering, 24(1) (**2012**) 92-101.

[45] Zaharaki, D., Galetakis, M. and Komnitsas, K., Valorization of construction and demolition (C&D) and industrial wastes through alkali activation. Construction and Building Materials, 121 (**2016**) 686-693.

[46] Z. Li, L. Wang, G. Ma, Mechanical improvement of continuous steel microcable reinforced geopolymer composites for 3D printing subjected to different loading conditions, Composites Part B: Engineering, 187 (**2020**) 107796.

[47] M. Chougan, S.H. Ghaffar, M. Jahanzat, A. Albar, N. Mujaddedi, R. Swash, The influence of nano-additives in strengthening mechanical performance of 3D printed 93 multi-binder geopolymer composites, Construction and Building Materials, 250 (**2020**) 118928.

[48] S. Muthukrishnan, S. Ramakrishnan, J. Sanjayan, Effect of alkali reactions on the rheology of one-part 3D printable geopolymer concrete, Cement and Concrete Composites, 116 (**2020**) 103899.

[49] G. Ma, Z. Li, L. Wang, F. Wang, J. Sanjayan, Mechanical anisotropy of aligned fiber reinforced composite for extrusion-based 3D printing, Construction and Building Materials, 202 (**2019**) 770-783.

[50] Davidovits, J., Chemistry of geopolymeric systems, terminology. In Geopolymer, 99(292) (**1999**) 9-39.

[51] T. Wohlers, T. Gornet, History of additive manufacturing, Wohlers report, 24 (**2014**)118.

[52] M. Shellabear, O. Nyrhilä, DMLS-Development history and state of the art, Proceedings of the 4th LANE 2004, Sept. 22.-24, (**2004**).

[53] L. Yang, K. Hsu, B. Baughman, D. Godfrey, F. Medina, M. Menon, S. Wiener, Additive manufacturing of metals: the technology, materials, design and production, (**2017**).

[54] M. Gouge, P. Michaleris, Thermo-mechanical modeling of additive manufacturing, Butterworth-Heinemann (**2017**).

[55] ASTMF2792-12a, Standard terminology for additive manufacturing technologies, ASTM International, (**2012**)

[56] Lloret, E., Shahab, A. R., Linus, M., Flatt, R. J., Gramazio, F., Kohler, M. and Langenberg, S., Complex concrete structures: Merging existing casting techniques with digital fabrication. Computer-Aided Design, 60 (**2015**) 40-49.

[57] T. Wangler, E. Lloret, L. Reiter, N. Hack, F. Gramazio, M. Kohler, M. Bernhard, B. Dillenburger, J. Buchli, N. Roussel, Digital concrete: opportunities and challenges, RILEM Technical Letters, 1 (**2016**) 67-75.

[58] Perrot, A., Rangeard, D. and Pierre, A., Structural built-up of cement-based materials used for 3D-printing extrusion techniques. Materials and Structures, 49(4) (**2016**) 1213-1220.

[59] Shakor, P., Sanjayan, J., Nazari, A. and Nejadi, S., Modified 3D printed powder to cement-based material and mechanical properties of cement scaffold used in 3D printing. Construction and Building Materials, 138 (**2017**) 398-409.

[60] J. Biernacki, J. Bullard, G. Sant, K. Brown, F. Glasser, S. Jones, M. Ley, R. Livingston, L. Nicoleau, J. Olek, F. Sanchez, R. Shahsavari, P. Stutzman, K. Sobolev, T. Prater, Cements in the 21 st Century: Challenges, Perspectives, and Opportunities, Journal of the American Ceramic Society, 100 (**2017**).

[61] Cesaretti, G., Dini, E., De Kestelier, X., Colla, V. and Pambaguian, L., Building components for an outpost on the Lunar soil by means of a novel 3D printing technology. Acta Astronautica, 93 (**2014**) 430-450

[62] R.A. Buswell, R.C. Soar, A.G. Gibb, A. Thorpe, Freeform construction: mega-scale rapid manufacturing for construction, Automation in construction, 16 (**2007**) 224-231.

[63] Le, T.T., Austin, S.A., Lim, S., Buswell, R.A., Gibb, A.G. and Thorpe, T., Mix design and fresh properties for high-performance printing concrete. Materials and Structures, 45(8) (**2012**) 1221-1232

[64] Panda, B., Paul, S. C., Mohamed, N. A. N., Tay, Y. W. D. and Tan, M. J., Measurement of tensile bond strength of 3D printed geopolymer mortar. Measurement, 113 (**2018**) 108-116.

[65] Paul, S.C., Tay, Y.W.D., Panda, B. and Tan, M.J., Fresh and hardened properties of 3D printable cementitious materials for building and construction. Archives of Civil and Mechanical Engineering, 18 (1) (**2018**) 311-319.

[66] Lim, S., Buswell, R.A., Le, T.T., Austin, S.A., Gibb, A.G. and Thorpe, T., "Developments in construction-scale additive manufacturing processes. Automation in Construction, 21 (**2012**) 262-268.

[67] Tay, Y.W. D., Panda, B., Paul, S.C., Tan, M.J., Qian, S.Z., Leong, K.F. and Chua, C.K., Processing and properties of construction materials for 3D printing. In Materials Science Forum, 861 (**2016**) 177-181.

[68] S. Al-Qutaifi, A. Nazari, A. Bagheri, Mechanical properties of layered geopolymer structures applicable in concrete 3D-printing, Construction and Building Materials, 176 (**2018**) 690-699.

[69] B. Nematollahi, P. Vijay, J. Sanjayan, A. Nazari, M. Xia, V.N. Nerella, V.Mechtcherine, Effect of Polypropylene Fibre Addition on Properties of Geopolymers Made by 3D Printing for Digital Construction, Materials, 11 (**2018**) 2352.

[70] B. Nematollahi, M. Xia, J. Sanjayan, P. Vijay, Effect of type of fiber on inter-layer bond and flexural strengths of extrusion-based 3D printed geopolymer, Materials science forum, Trans Tech Publ, (**2018**), pp. 155-162.

[71] B. Nematollahi, M. Xia, P. Vijay, J.G. Sanjayan, Properties of extrusion-based 3D printable geopolymers for digital construction applications, 3D Concrete Printing Technology, Elsevier (**2019**), pp. 371-388.

[72] T. Ding, J. Xiao, S. Zou, X. Zhou, Anisotropic behavior in bending of 3D printed concrete reinforced with fibers, Composite Structures, 254 (**2020**) 112808.

[73] G. Ma, Z. Li, L. Wang, G. Bai, Micro-cable reinforced geopolymer composite for extrusion-based 3D printing, Materials Letters, 235 (**2019**) 144-147.

[74] B. Panda, G.H. Ting, A. Annapareddy, M. Li, Flow and mechanical properties of 3D printed cementitious material with recycled glass aggregates, **2018**.

[75] Y.W.D. Tay, G.H.A. Ting, Y. Qian, B. Panda, L. He, M.J. Tan, Time gap effect on bond strength of 3D-printed concrete, Virtual and Physical Prototyping, 14 (**2019**) 104-113.

[76] B. Panda, N.A. Noor Mohamed, Y.W.D. Tay, M.J. Tan, Bond strength in 3D printed geopolymer mortar, RILEM International Conference on Concrete and Digital Fabrication, Springer, (**2018**), pp. 200-206.

[77] Shang, J., Dai, J. G., Zhao, T. J., Guo, S. Y., Zhang, P. and Mu, B., Alternation of traditional cement mortars using fly ash-based geopolymer mortars modified by slag. Journal of Cleaner Production, 203 (**2018**) 746-756.

[78] Furtos, Gabriel, et al. "Mechanical and thermal properties of wood fiber reinforced geopolymer composites." Journal of Natural Fibers 19.13 (**2022**): 6676-6691.

[79] Arun R. Arunothayan, Behzad Nematollahi, Ravi Ranade, Shin Hau Bong, Jay G. Sanjayan, Kamal H. Khayat, Fiber orientation effects on ultra-high performance concrete formed by 3D printing,Cement and Concrete Research,Volume 143, (**2021**),106384.

[80] Bouaissi, A., Li, L. Y., Moga, L. M., Sandu, I. G., Abdullah, M. M. A. B. and Sandu, A. V., A review on fly ash as a raw cementitious material for geopolymer concrete. Rev. Chim, 69(7) (**2018**) 1661-1667.

[81] Ilcan, H., Sahin, O., Unsal, Z., Ozcelikci, E., Kul, A., & Cağatay Demiral, N. et al. (**2023**). Effect of industrial waste-based precursors on the fresh, hardened and environmental performance of construction and demolition wastes-based geopolymers. Construction And Building Materials, 394, 132265.

[82] Thang, N. H., Evaluation on Formation of Aluminosilicate Network in Ternary-Blended Geopolymer Using Infrared Spectroscopy. In Solid State Phenomena. Trans Tech Publications Ltd., 296 (**2019**) 99-104.

[83] Zailani, W. W. A., Abdullah, M. M. A., Arshad, M. F., Burduhos-Nergis, D. D. and Tahir, M. F. M., Effect of Iron Oxide (Fe2O3) on the Properties of Fly Ash Based Geopolymer. 161 In IOP Conference Series: Materials Science and Engineering. IOP Publishing, 877(1) (**2020**) 012017.

[84] Demiral, N., Ozkan Ekinci, M., Sahin, O., Ilcan, H., Kul, A., Yildirim, G., & Sahmaran, M. Mechanical anisotropy evaluation and bonding properties of 3D-printable construction and demolition waste-based geopolymer mortars. Cement And Concrete Composites, (**2022**). 134, 104814.

[85] S.H. Bong, M. Xia, B. Nematollahi, C. Shi, Ambient temperature cured ‘just-addwater’ geopolymer for 3D concrete printing applications, Cement and Concrete Composites, 121 (**2021**) 104060.

[86] Provis, J.L., Bernal, S.A. Geopolymers and Related Alkali-Activated Materials. Annual Review of Materials Research (**2014**), 44, 299-327.

[87] Palomo, A., Fernández-Jiménez, A., Criado, M. Alkali-activated cementitious materials: Alternative matrices for the immobilization of hazardous wastes. Part I. Stabilization of boron waste. Cement and Concrete Research (**2006**), 36(2), 189-195.

[88] Temuujin, J., Van Riessen, A., Williams, R. Influence of Ca(OH)2 concentration on mechanical and microstructural development of fly ash geopolymer pastes. Journal of Materials Science (**2009**), 44(5), 1357-1366.

[89] Temuujin, J., Minjigmaa, A., Rickard, W., Lee, M., Lee, J.Y. Influence of NaOH solution concentration on the mechanical and microstructural characteristics of fly ash-based geopolymers. Ceramics International, (**2015**). 41(10), 14566-14573.

[90] Bernal, S.A., Provis, J.L., Walkley, B., San Nicolas, R., Gehman, J.D., Brice, D.G., Kilcullen, A.R., Duxson, P. Gel nanostructure in alkali-activated binders based on slag and fly ash, and effects of accelerated carbonation. Cement and Concrete Research, (**2012**). 42(6), 885-891.

[91] Temuujin, J. V., Van Riessen, A. and Williams, R., Influence of calcium compounds on the mechanical properties of fly ash geopolymer pastes. Journal of hazardous materials, 167(1-3) (**2009**) 82-88.

[92] Palomo, A., Grutzeck, M.W., Blanco, M.T. Alkali-activated fly ashes. A cement for the future. Cement and Concrete Research, (**1999**). 29(8), 1323-1329

[93] Tuğluca, M., Özdoğru, E., İlcan, H., Özçelikci, E., Ulugöl, H., & Şahmaran, M. Characterization of chemically treated waste wood fiber and its potential application in cementitious composites. Cement And Concrete Composites, (**2023**). 137, 104938.

[94] Z. Zuhua, Y. Xiao, Z. Huajun, C. Yue, Role of water in the synthesis of calcined kaolin-based geopolymer, Applied Clay Science, 43 (**2009**) 218-223.

[95] W.M. Kriven, J.L. Bell, M. Gordon, Microstructure and microchemistry of fully-reacted geopolymers and geopolymer matrix composites, Ceramic Transactions, 153 (**2003**) 227-250.

[96] M. Lizcano, A. Gonzalez, S. Basu, K. Lozano, M. Radovic, Effects of water content and chemical composition on structural properties of alkaline activated metakaolin-based geopolymers, Journal of the American Ceramic Society, 95 (**2012**) 2169-2177.

[97] De Schutter, G., Lesage, K., Mechtcherine, V., Nerella, V. N., Habert, G. and AgustiJuan, I., Vision of 3D printing with concrete—Technical, economic and environmental potentials. Cement and Concrete Research, 112 (**2018**) 25-36.

[98] Panda, B., Paul, S. C., Mohamed, N. A. N., Tay, Y. W. D. and Tan, M. J., Measurement of tensile bond strength of 3D printed geopolymer mortar. Measurement, 113 (**2018**) 108-116.

[99] B. Nematollahi, M. Xia, P. Vijay, J.G. Sanjayan, Properties of extrusion-based 3D printable geopolymers for digital construction applications, 3D Concrete Printing Technology, Elsevier (**2019**), pp. 371-388.

[100] Afroughsabet, V., Biolzi, L., & Ozbakkaloglu, T. High-performance fiber-reinforced concrete: a review. Journal of materials science, (**2016**). 51, 6517-6551.

[101] Zollo, R. F. Fiber-reinforced concrete: an overview after 30 years of development. Cement and concrete composites, (**1997**). 19(2), 107-122.

[102] Bartos, P. J. M., & Duris, M. Inclined tensile strength of steel fibres in a cement-based composite. Composites, (**1994**). 25(10), 945-952.

[103] C. Li, V. Postcrack scaling relations for fiber reinforced cementitious composites. Journal of materials in civil engineering, (**1992**). 4(1), 41-57.

[104] Li, V. C., Stang, H., & Krenchel, H. Micromechanics of crack bridging in fibre-reinforced concrete. Materials and structures, (**1993**). 26, 486-494.

[105] Tran, T. T., Pham, T. M., & Hao, H. Experimental and analytical investigation on flexural behaviour of ambient cured geopolymer concrete beams reinforced with steel fibers. Engineering Structures, (**2019**). 200, 109707.

[106] Singh, A. P., & Singhal, D. Effect of fibre shapes on compressive and bond strengths of steel fibre reinforced concrete. Journal-institution of engineers india part cv civil engineering division, (**1998**). 79, 136-139.

[107] Zhang, P., Han, X., Zheng, Y., Wan, J., & Hui, D. Effect of PVA fiber on mechanical properties of fly ash-based geopolymer concrete. Reviews on advanced materials science, (**2021**). 60(1), 418-437.

[108] Xu, F., Deng, X., Peng, C., Zhu, J., & Chen, J. Mix design and flexural toughness of PVA fiber reinforced fly ash-geopolymer composites. Construction and Building Materials, (**2017**). 150, 179-189.

[109] Lowry, D. R., & Kriven, W. M. Effect of high tensile strength polypropylene chopped fiber reinforcements on the mechanical properties of sodium based geopolymer composites. Strategic Materials and Computational Design: Ceramic Engineering and Science Proceedings, (**2010**). 31, 47-56

[110] A.U. Rehman, J.-H. Kim, 3D concrete printing: A systematic review of rheology, mix designs, mechanical, microstructural, and durability characteristics, Materials, 14 (**2021**) 3800.

[111] H. Wang, H. Li, F. Yan, Synthesis and mechanical properties of metakaolinitebased geopolymer, Colloids and Surfaces A: Physicochemical and Engineering Aspects, 268 (**2005**) 1-6.

[112] T. Ding, J. Xiao, S. Zou, J. Yu, Flexural properties of 3D printed fibre-reinforced concrete with recycled sand, Construction and Building Materials, 288 (**2021**) 123077.

[113] T. Marchment, J.G. Sanjayan, B. Nematollahi, M. Xia, Interlayer strength of 3D printed concrete: influencing factors and method of enhancing, 3D concrete printing technology, Elsevier, (**2019**), pp. 241-264.

[114] S. Muthukrishnan, S. Ramakrishnan, J. Sanjayan, Effect of alkali reactions on the rheology of one-part 3D printable geopolymer concrete, Cement and Concrete Composites, 116 (**2020**) 103899

[115] V. Mechtcherine, V.N. Nerella, F. Will, M. Näther, J. Otto, M. Krause, Large-scale digital concrete construction – CONPrint3D concept for on-site, monolithic 3D-printing, Automation in Construction, 107 (**2019**) 102933.

[116] T. Ding, J. Xiao, S. Zou, X. Zhou, Anisotropic behavior in bending of 3D printed concrete reinforced with fibers, Composite Structures, 254 (**2020**) 112808.

[117] G. Ma, Z. Li, L. Wang, G. Bai, Micro-cable reinforced geopolymer composite for extrusion-based 3D printing, Materials Letters, 235 (**2019**) 144-147.

[118] H. Ilcan, O. Sahin, A. Kul, G. Yildirim, M. Sahmaran, Rheological properties and compressive strength of construction and demolition waste-based geopolymer mortars for 3D-Printing, Construction and Building Materials, 328 (**2022**) 127114.

[119] O. Şahin, H. İlcan, A.T. Ateşli, A. Kul, G. Yıldırım, M. Şahmaran, Construction and demolition waste-based geopolymers suited for use in 3-dimensional additive manufacturing, Cement and Concrete Composites, 121 (**2021**) 104088.

[120] T.T. Le, S.A. Austin, S. Lim, R.A. Buswell, R. Law, A.G.F. Gibb, T. Thorpe, Hardened properties of high-performance printing concrete, Cement and Concrete Research, 42 (**2012**) 558-566.